PRESSURE DEPENDENCE OF SUPERCONDUCTING PROPERTIES OF MgB_2

By

Henrich Ploczek

Mgr. (Physics) Comenius University,

Bratislava, Slovak Republic

A THESIS SUBMITTED IN PARTIAL FULFILLMENT OF

THE REQUIREMENTS FOR THE DEGREE OF

MASTER OF SCIENCE

in

THE FACULTY OF MATHEMATICS AND SCIENCE

DEPARTMENT OF PHYSICS

BROCK UNIVERSITY

April 2003

Table of Contents

List of Tables

List of Figures

Abstract

We prepared samples of MgB_2 and ran sets of experiments aimed for investigation of superconducting properties under pressure. We found the value of pressure derivative of the transition temperature -1.2 ± 0.05 K/GPa. Then, using McMillan formula, we found that the main contribution to the change of the transition temperature under the pressure is due to the change in phonon frequencies. Grüneisen parameter was calculated to be $\gamma_G = 2.4$. Our results suggest that MgB_2 is a conventional superconductor.

Acknowledgement

I would like to thank my supervisor Dr. F. S. Razavi for his help and support, which enabled me to complete my research.

I would also like to thank Dr. S. K. Bose for his valuable discussions about the theoretical part of this work and to members of my committee, Dr. B. Mitrović and Dr. D. A. Crandles for carefully reading this thesis and making suggestions.

My sincere appreciation to the machine shop, electronics shop and the glassblower for all their help.

My thanks also to Dr. E. Sternin for his help in mastering LaTeX.

Chapter 1

Introduction

The beginning of research on superconductivity in MgB_2 dates back to January 2001 when Akimitsu et al. [1] reported the discovery of superconductivity in this material. This was really unexpected, because MgB_2 is not a new material. It had been known and industrially used since the early 1950s. What was surprising was the relatively high superconducting transition temperature of 39 K. There are many superconductors with much higher transition temperatures. But not many of them are as cheap and as easy to fabricate, which is one of the advantages of magnesium di-boride (high T_c cuprates, for example, are difficult to fabricate and they are expensive since HTSC wires are 70% silver).

Another advantage of MgB_2 is that the T_c is above the temperature of boiling hydrogen ($\sim$ 21 K). This allows refrigerating systems without the need of expensive liquid helium. It has larger coherence lengths than cuprates and the critical current is not limited by grain boundaries [6]. It is for all these reasons that attempts are made to improve its properties, especially the transition temperature, in order to be used in technical applications.

High hopes were put into this material as it was expected that it was just the tip of an iceberg of a new family of superconductors with higher T_c and a search for similar materials and for possible substitutions started. Lighter elements have higher phonon frequencies. Higher phonon modes do not necessarily mean an increase in T_c, but was

considered as one of the ways how to increase T_c and could be done by doping. Theoretical calculations were optimistic in terms of the possibility to increase the transition temperature this way, even exceeding the temperature of boiling nitrogen [24]. Although experimental attempts were made, only few elements (Al, Li) substitute on the Mg site [27, 28, 48]. For the boron site, carbon doping was reported with varying results [26, 29, 30, 31, 32, 33, 34]. Because of difficulties with doping by traditional solid-state synthesis, electrochemical doping was suggested [25]. Now it appears that MgB_2 is the one with the best possible combination of parameters (responsible for the value of T_c) of this class of materials as shown in the Table 1.1.

Compound	T_c (K)	Reference
TaB_2	9.5	[24]
ZrB_2	5.5	[24]
$Mg_{0.95}Zn_{0.05}B_2$	38	[24]
$Mg_{0.97}Zn_{0.03}B_2$	38.4	[24]
$Mg_{0.99}Al_{0.01}B_2$	38	[28]
$Mg_{0.90}Al_{0.10}B_2$	36	[28]
$Mg_{0.90}Ca_{0.10}B_2$	38	[28]
$Mg_{0.90}Cu_{0.10}B_2$	38.5	[28]
$Mg_{0.95}Zn_{0.05}B_2$	39	[28]
$Mg_{0.80}Zn_{0.20}B_2$	38	[28]
$Mg_{0.90}Ag_{0.10}B_2$	38.5	[28]
MgB_2	39	[1]

Table 1.1: **Transition temperatures of similar materials and doped MgB_2. In all cases T_c is lower than the transition temperature of pure MgB_2.**

High critical temperatures for a metallic compound raised the question of whether MgB_2 is a conventional or non-conventional superconductor. Some of its properties are conventional (e.g. isotope effect [18, 19], linear temperature dependence of the upper critical field with a positive curvature near T_c [17] etc.), while some are closer to the behavior of non-conventional superconductors (quadratic temperature dependence of penetration

depth [20, 21, 22], sign reversal of the Hall effect near T_c [23]).

MgB_2 can be prepared as single crystals (which are up to date very small), polycrystalline bulk samples, polycrystaline powders, wires, tapes and thin films, depending on the preparation method used. The method also determines, whether the bulk samples are dense (as prepared by high pressure – high temperature method [15, 28] or by reactive liquid Mg infiltration [13]) or porous (prepared by standard solid state reaction) [15, 28, 40].

The purpose of this work was to prepare MgB_2 and to study pressure dependence of the superconducting transition temperature and normal state resistivity from magnetization and resistance measurements. The obtained slope (dT_c/dP) was then used in theoretical models [8, 11] to determine Grüneisen prameter and this result was compared with results of other researchers groups working on the same subject.

The pure MgB_2 sample we fabricated had excess of nonreacted Mg, as concluded from x-ray diffraction measurements. At the time of preparation it was suggested to add an extra 5-10% of magnesium [41], which later was shown to be unnecessary.

In this work we will first describe some basic properties of superconductors and qualitatively investigate pressure effects on the resistivity and the transition temperature. In experimental part we will describe our apparatus, the methods we used to produce samples and measurement procedures. In the analysis of results we will look at the crystal structure of our samples using x-ray diffraction, we will make some remarks about resistivity measurements results and finally, we will use theoretical models to show that MgB_2 is a conventional BCS superconductor.

Chapter 2

Properties of superconductors

2.1 Zero resistance

In 1911, three years after liquidifying helium, H. Kamerlingh-Onnes discovered that the resistance of mercury, when cooled to temperature 4.15 K, drops to zero. Further research showed that other metals and alloys also exhibit this property, called superconductivity. By measuring changes in magnetic field created by supercurrents, which are induced by magnetic field applied to a superconductor, we can estimate that these currents circulate in the specimen for many years, in some special cases as much as 10^{10} years. The temperature of transition between superconducting and normal phase, the critical temperature T_c, is characteristic for every material and varies from very low temperatures well below 1 K up to above 133 K in high T_c superconductors.

2.2 Meissner effect

After the discovery of superconductivity another property was found - superconductors are also perfect diamagnets. That is, they completely exclude all magnetic field from their interior, therefore the magnetic flux inside the superconductor is zero (Figure 2.1a). If the magnetic field is applied onto a specimen at the temperature $T > T_c$, it penetrates the specimen like a normal nonmagnetic material as shown in the Figure 2.1b. Now if we cool down the sample below the transition temperature, the situation changes, because

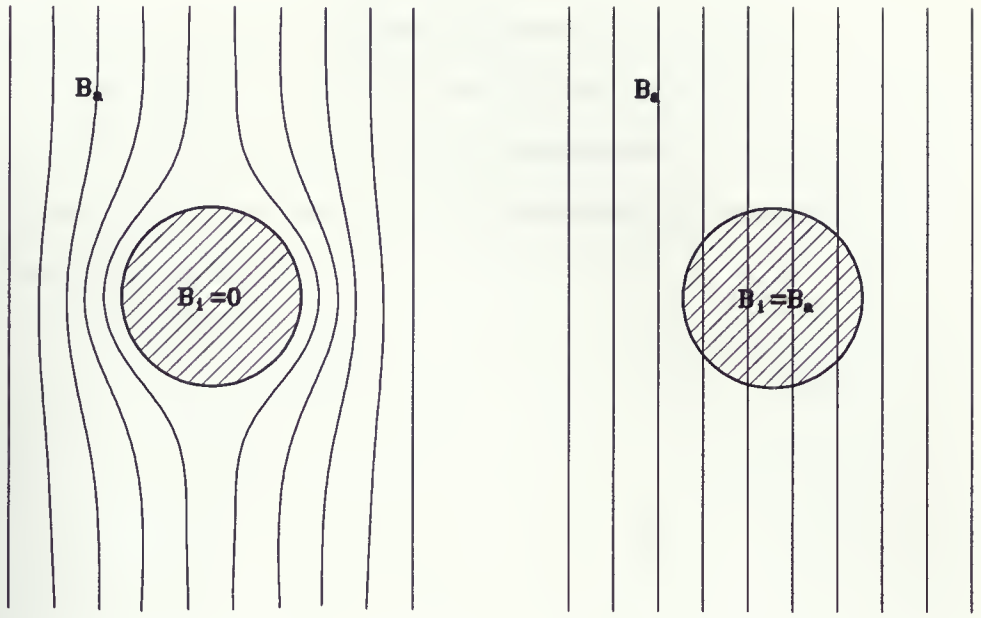

(a) (b)

Figure 2.1: **Meissner effect: (a)** $T < T_c$ **and** $B < B_c$**, (b)** $T > T_c$ **and** $B > B_c$**.**

the magnetic field is pushed out of the specimen. The internal field $B_i = 0$, then

$$\mu_0 H + \mu_0 M = B_i = 0$$

from which

$$\frac{M}{H} = \chi = -1$$

where H is the intensity of a magnetic field and M is magnetization. It has to be said that this property of perfect diamagnetism is not a consequence of Maxwell equations. If $\rho = 0$ then, from Ohm's law, $\vec{E}$ has to be zero as well. Then we know that $\vec{\nabla} \times \vec{E} = d\vec{B}/dt$. This only means that the magnetic flux B is constant, it does not say that it is zero. So zero resistivity is not the cause of the Meissner effect.

Although superconductors are perfect diamagnets, the origin of this diamagnetism is not atomic, as it is in "normal" diamagnets, instead, it is a consequence of compensation

of the magnetic field inside the material by surface electron currents, which arise when magnetic field is applied. The superconductivity can be destroyed by external magnetic fields. This critical magnetic field H_c is temperature dependent as shown in the Figure 2.2 Below the curve $H_c(T)$, the material is in superconducting state, above the curve it is in normal state (Figure 2.2).

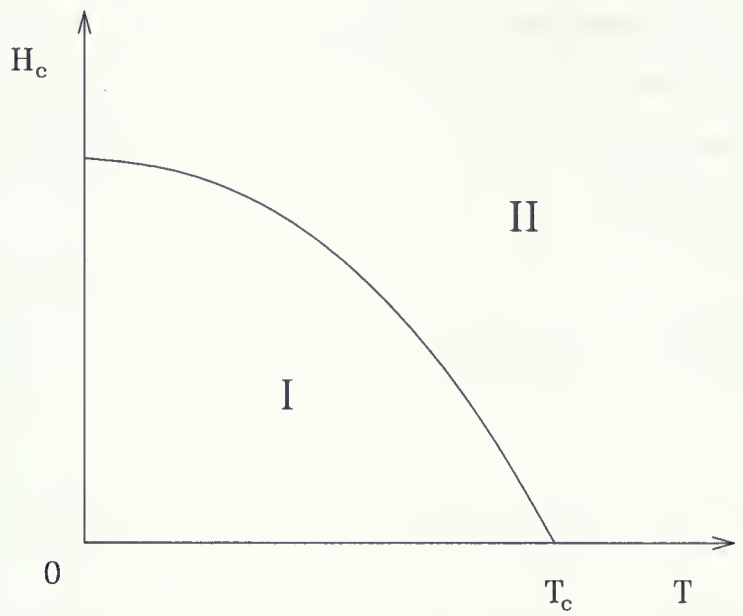

Figure 2.2: **Critical magnetic field as a function of temperature. Region I: superconducting state, region II: normal state.**

Generally, there are two groups of superconductors: type I, which show behavior described above, and type II, which are characterized by the existence of a mixed or vortex state, in addition to the normal and Meissner states. In this state the magnetic field partially penetrates the specimen, while the material is still superconducting. The boundary curve between the mixed state and the Meissner state is called lower critical field H_{c1}, the boundary curve between the mixed state and the normal state is called higher critical field H_{c2}.

Since the current creates a magnetic field, even superconducting current can create

field which is high enough to destroy superconductivity. This current is called the critical current density j_c.

From a microscopic point of view, superconductivity was successfully described by the theory of Bardeen, Cooper and Schriefer, known as BCS theory [46]. It is based on the attractive interaction between electrons, which causes all electrons to form pairs. The pair has lower energy than two single electrons. The scattering by the phonons can occur only if the energy given to the pair by the lattice is high enough to break the pair.

The vortex (mixed) state is characterized by vortices – tiny tubes in normal state, surrounded by regions in superconducting state. These vortices disappear when the external field reaches the higher critical field.

More details about the theory of superconductivity can be found in *Superconductivity* [47]

2.3 Pressure effects

Studies of the effects that pressure has on superconducting properties, particularly the transition temperature, are very important for various reasons. First of all, the value of dT_c/dP can help to modify the superconductor to obtain higher T_c's. High pressure studies can also help to create new superconductors, vary properties of already known superconductors, induce structural phase transitions and vary lattice parameters to test theoretical models.

In an ideal case, the pressure applied to the specimen would be purely hydrostatic, thus the properties of a superconductor would reflect changes in lattice parameters. In most cases, however, the pressure is not hydrostatic. This is due to the fact that the pressure-transmitting medium, a fluid at room temperature, freezes at a certain temperature and introduces a shear stress. This stress can then cause deformations and lattice defects. An important factor, in terms of $T_c(P)$ measurements, is whether the pressure medium freezes above or below the transition temperature. The only pressure transmitting medium, which can be considered as capable of maintaining hydrostatic character throughout the whole temperature range is helium. Even though helium freezes (it remains fluid at $T_c \simeq 39$ K up to 0.5 GPa), it is, in its solid form, the softest material known. However, all this depends also on the rate of cooling because even if the pressure transmitting medium is frozen, if cooled slowly, the pressure can be very close to hydrostatic. On the other hand even helium, if cooled improperly, may introduce sheer stress as well.

2.3.1 Effect of pressure on resistivity

The transport properties of solids, in general, are described by the Boltzmann equation. The motion of carriers in solids is affected by external fields and scattering by impurities

and phonons. For electrical conductivity, we consider only the presence of an electric field. Solving the Boltzmann equation for these conditions and some simplifications give us the general formula for conductivity [49] :

$$\overline{\overline{\sigma}} = \frac{1}{4\pi^3}\frac{e^2}{\hbar}\int \frac{\vec{v_k}\vec{v_k}dS_F}{v_{\vec{k}}} \tag{2.1}$$

where $\overline{\overline{\sigma}}$ is a tensor, $\vec{v_k}$ is the velocity of a carrier in state $\vec{k}$ and dS_F is an element of the Fermi surface. The kinetic method of dealing with transport properties leads to:

$$\sigma = \frac{ne^2\tau}{m} \tag{2.2}$$

where n is the number of free carriers, m is the mass of a carrier and τ is the relaxation time. This result is appropriate for a semiconductor, but for a metal, it is better to write:

$$\sigma = \frac{1}{3}j_F^2\tau N(0) \tag{2.3}$$

where

$$j_F = ev_F = e\left|\nabla_{\vec{k}}\mathcal{E}_{\vec{k}}\right|_{FS}$$

(the subscript FS denotes the Fermi surface average), v_F is the Fermi velocity and $N(0)$ is the density of states at the Fermi level. This shows that the electronic properties of metals are determined only by electrons at the Fermi surface.

Now we want to find the pressure dependence of quantities entering this equation. For investigating pressure effects we use the connection between pressure and volume – when pressure is applied to the specimen, its volume decreases. We will use a simplified picture, an analogy for which a qualitative description might be sufficient. In general, for calculating $\left|\nabla_{\vec{k}}\mathcal{E}_{\vec{k}}\right|_{FS}$ we would have to know the Fermi surface. Therefore determining the Fermi velocity (and its pressure dependence) would be a difficult task. But if we believe that the material is free-electron like, we can use the free-electron model. MgB_2

behaves to some extent as a free-electron metal (typical *sp* metal), with B–B bonding being more covalent (directional) rather than metallic. Now we can use the example of an electron in a box. The energy levels of that electron depend on box dimensions. By decreasing the volume, energy levels rise and since this energy is kinetic, the velocity of the electron increases as well. Therefore, in general, the term j_F^2 increases with pressure. It has to be kept in mind, however, that electrons in a real solid are not free, they "see" the periodic potential of the lattice. Smaller interatomic distances cause a larger overlap of electron orbitals and hopping from orbital to orbital is easier. This effect therefore causes an increase in electrical conductivity for higher pressures.

On the other hand, σ also depends on the density of states at the Fermi level $N(0)$. To find out the pressure dependence of this quantity, we have to realize that by applying pressure, the Fermi level is shifted to higher energies, while all the bands are broadened (i.e. valence band is broader). The broadening of the bands should cause the density of states to decrease with pressure, however, the value at the Fermi level depends on the position of the Fermi level with respect to nearby structural details (e.g. van Hove singularities, local maxima or minima). This means that $N(0)$ can in some cases increase.

The relaxation time τ is also a problem, because it is difficult to calculate, but we can expect that the relative change with pressure is smaller than that of the Fermi electron velocity and density of states at Fermi level. This is because the relaxation time is already very short in polycrystalline materials due to the large number of impurities.

For the free-electron model the pressure dependence of $j_F^2\tau$ is stronger than the pressure dependence of $N(0)$. This is because for the free-electron gas, the function j_F^2 is proportional to k_F^2, $N(0)$ is proportional to k_F and wave vector k_F is proportional to $V^{-1/3}$. Thus, according to equation 2.3, in most cases the resistivity would decrease with pressure.

2.3.2 Effect of pressure on transition temperature

Conventional superconductors are well described by BCS theory of superconductivity [47]. The original equation for calculating the transition temperature is:

$$T_c = 1.14\,\Theta_D \exp\left[-\frac{1}{\lambda}\right] \tag{2.4}$$

where $\lambda = N(0)V$ is the product of density of states at Fermi level $N(0)$ and pairing potential V. Θ_D is the Debye temperature (proportional to $\langle\omega^2\rangle^{1/2}$). This relation is valid for $\lambda < 1/4$.

To illustrate how vibrational modes of the lattice are affected by the pressure, we can look at a solid as a set of oscillating atoms placed in a periodic lattice. These atoms are connected to their nearest neighbors by "springs" (this is a consequence of the nature of the binding potential). Applying pressure means a decrease in average interatomic distances, accompanied by deformation of the binding potential and stiffening of the springs. This in turn increases oscillation (vibrational) frequencies.

As mentioned previously, the density of states is unique for each material and its value at Fermi level cannot be easily predicted in general. This value depends on the position of the Fermi level as it changes with pressure.

From an experimental point of view, there was a discrepancy in the relation between the transition temperature and the superconducting gap parameter ($2\Delta(0)/kT_c = 3.53$) for some strongly coupled superconductors (e.g. Pb, Hg). For this reason, inelastic phonon processes were taken into account and some modifications were made. McMillan [43] used Eliashberg equations [45] and extended results for strong-coupling superconductors:

$$T_c = \frac{\Theta_D}{1.45} \exp\left[-\frac{1.04(1+\lambda)}{\lambda - \mu^*(1+0.62\lambda)}\right] \tag{2.5}$$

Here μ^* is the Coulomb pseudopotential. This equation was found to be very accurate

for materials with $\lambda < 1.5$. However, the equation was then reanalyzed and altered by Allen [44] for very large λ:

$$T_c = \frac{\langle \omega_{ln} \rangle}{1.2} \exp\left[-\frac{1.04(1+\lambda)}{\lambda - \mu^*(1+0.62\lambda)} \right] \tag{2.6}$$

where $\langle \omega_{ln} \rangle$ is logarithmically averaged phonon frequency[1]. This is a phenomenological equation and although it is derived from Eliashberg equations, it is not an exact solution, but it is very accurate for most conventional superconductors.

To express this equation as an explicit function of pressure, we can use the procedure proposed by Chen et al. [8]. First, we introduce quantities:

$$\gamma_G = -\frac{\partial \ln \langle \omega^2 \rangle^{1/2}}{\partial \ln V} \approx -\frac{\partial \ln \langle \omega_{ln} \rangle}{\partial \ln V} \tag{2.7}$$

$$\varphi = \frac{\partial \ln \lambda}{\partial \ln V} \tag{2.8}$$

$$\phi = \frac{\partial \ln \mu^*}{\partial \ln V} \tag{2.9}$$

These quantities can be integrated:

$$\langle \omega_{ln} \rangle (V) = \langle \omega_{ln} \rangle (V_0) \left(\frac{V}{V_0} \right)^{-\gamma_G} \tag{2.10}$$

$$\lambda(V) = \lambda(V_0) \left(\frac{V}{V_0} \right)^{\varphi} \tag{2.11}$$

$$\mu^*(V) = \mu^*(V_0) \left(\frac{V}{V_0} \right)^{\phi} \tag{2.12}$$

where V is a unit-cell volume at applied pressure, V_0 is a unit-cell volume at ambient pressure. Now we use Murnaghan equation of state $V(P) = V(0)(1 + B'P/B)^{-1/B'}$ in order to get:

$$\langle \omega_{ln} \rangle (P) = \langle \omega_{ln} \rangle (0) \left(1 + \frac{B'}{B} P \right)^{\frac{\gamma_G}{B'}} \tag{2.13}$$

$$\lambda(P) = \lambda(0) \left(1 + \frac{B'}{B} P \right)^{-\frac{\varphi}{B'}} \tag{2.14}$$

[1]The logarithmically averaged phonon frequency is defined as $\exp \langle \ln \omega \rangle$.

$$\mu^*(P) = \mu^*(0)\left(1+\frac{B'}{B}P\right)^{-\frac{\phi}{B'}} \tag{2.15}$$

These results can then be substituted into the McMillan formula (Equation 2.6), which will become an explicit function of pressure:

$$T_c(P) = T_c[\langle\omega_{ln}\rangle(P), \lambda(P), \mu^*(P)] \tag{2.16}$$

Thus if we manage to fit this function to the experimental data, it can both test the theoretical model and provide the evidence that the investigated material is a conventional superconductor.

Chapter 3

Experimental setup

3.1 Pressure cells

Application of pressure to the sample was performed by using so-called pressure cells. For different purposes, we used different pressure cell designs. The basic idea is always the same: pressure applied in the hydraulic press is transferred to the specimen through a pressure medium and is locked by a nut on the cell. We used two types of pressure cells: a hydrostatic pressure cell (HPC) and a quasi-hydrostatic pressure cell (QHPC). The difference between these two is the pressure medium used. To determine the pressure inside the cell, an internal Pb manometer was used. The pressure dependencies of transition temperature and resistivity of Pb are calibrated. For our experiments, we used three pressure cells: two for hydrostatic pressure (magnetization and resistivity measurements) and one for quasi-hydrostatic (resistance measurements).

All pressure cells were made of copper beryllium, which is a strong material with a high thermal capacity necessary for a slow uniform temperature change during the warm up while the experiment is running. Some parts, however, are made of tungsten carbide and hardened steel.

HPC for magnetization measurements was specially designed (by F. S. Razavi) for SQUID magnetometer (Figure 3.1). Since there is no need for wires to be attached to the specimen, the design is somewhat easier than the standard HPC. As a pressure transmitting medium, silicon oil was used. There is no internal thermometer in this cell,

the temperature is monitored by the SQUID magnetometer control system. To assemble the cell, nylon container (G) is carefully filled with silicon oil, so that no air bubbles stay inside and a very small piece of specimen and lead are inserted. Then, the container is connected to the plug (I), which is then inserted into the cell and the nut (C) is tightened. From the other side of the cell, a piece of sapphire (F) and the plug (E) are inserted. The nut (B) is tightened. To apply pressure, the cell is put into a special holder and required force[1] is applied to the piston rod (D). Then, the nut (B) is tightened, the force is released and the piston rod (D) is removed. The pressure is "locked" inside and the cell is ready for measurement.

In the case of HPC for resistivity measurements, 1:1 solution of 2-methyl butane and 3-methyl-1-butanol as a pressure transmitting medium, was used. The schematic drawing is shown in the Figure 3.2. The function is in principle the same, the only difference is in the obturator (Figure 3.2: part H), which has electrical leads attached to it to allow a connection between the sample/lead and the measurement system. These leads are then drawn outside the cell through the cavity in the tightening nut (C). To assemble the cell, the nylon container (L) is filled with pressure transmitting medium and connected to the obturator (H), which has specimen and lead ribbon already attached to it. Then the cell is assembled the same way as the previous one.

The quasi-hydrostatic pressure cell is shown in the Figure 3.3. The specimen is placed between parts F and G. Electrical leads are drawn through the hole inside the anvil G and then through cavities in parts H and A.

[1]We applied usually up to 15 - 20 t (147 - 196 kN), where we started from zero and then we were gradually increasing the value for each next measurement.

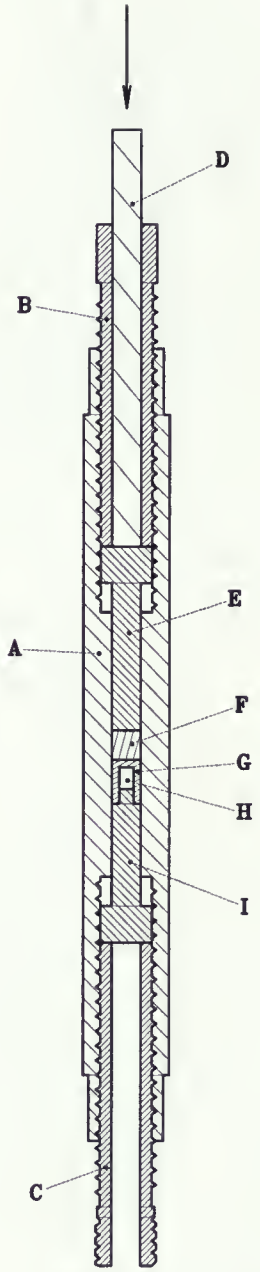

Figure 3.1: **Hydrostatic pressure cell for magnetization measurements: A – body of cell (CuBe); B, C – tightening nuts (CuBe); D – piston rod (WC); E – plug (CuBe); F – sapphire (Al_2O_3); G – nylon container; H – sample area; I – plug (CuBe). The arrow shows where the force is applied.**

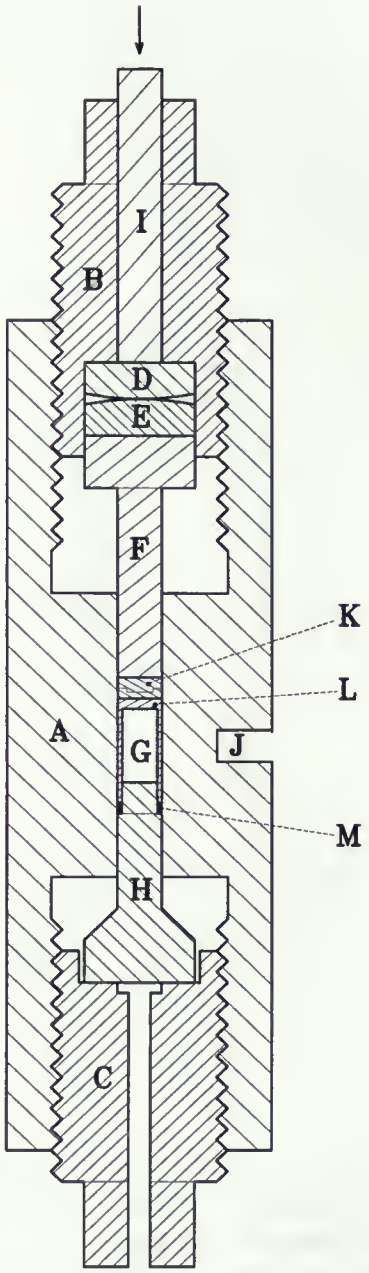

Figure 3.2: **Hydrostatic pressure cell for resistivity measurements: A – body of cell (CuBe); B, C – tightening nuts (CuBe); D, E – springs (CuBe); F – plug (CuBe/WC); G – sample area; H – obturator (hardened steel); I – piston rod (WC); J – thermometer area; K – protecting washer (CuBe/Teflon); L – nylon container; M – washer (CuBe). The arrow indicates where the force is applied.**

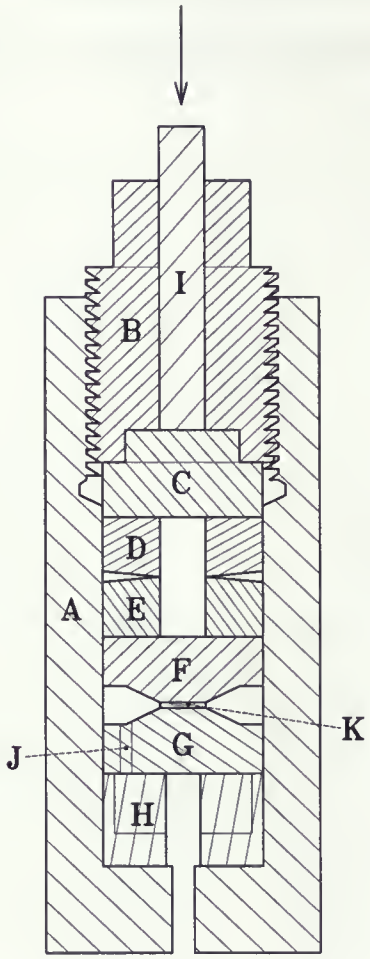

Figure 3.3: **Quasi-hydrostatic pressure cell: A – body of cell (Cu-Be); B – tightening nut (Cu-Be); C – pressure transmitting plug (hardened steel); D, E – springs (Cu-Be); F, G – anvils (CuBe/WC); H – wire protecting holder (Cu-Be); I – piston rod (WC); J – thermometer area; K – sample area (soapstone washer with the specimen inside). The arrow indicates, where the force is applied.**

3.1.1 Resistivity measurement system

This system was used for resistance (quasi-hydrostatic pressure) and resistivity (hydrostatic pressure) measurements. It consists of a four-chambered dewar (Figure 3.4), three constant current sources, several voltmeters and a computer used to control the experiment.

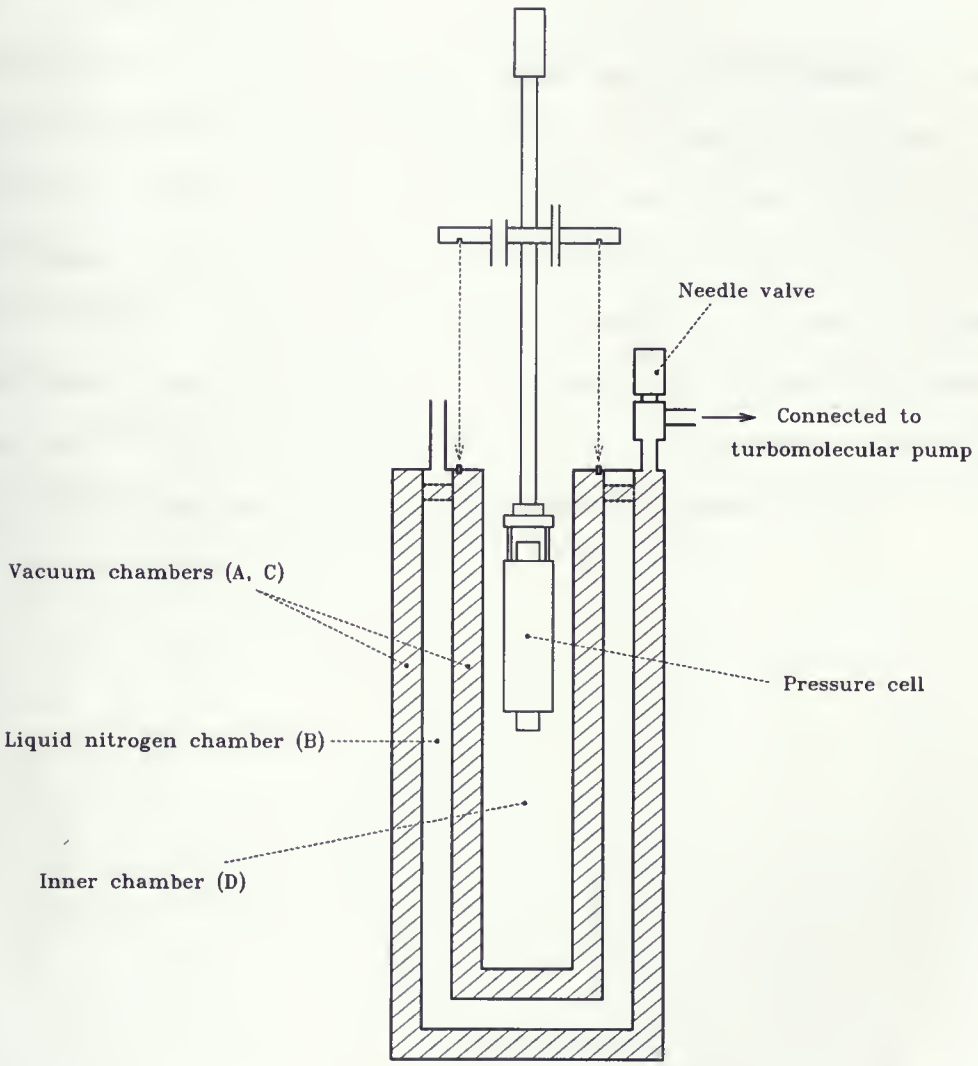

Figure 3.4: **Dewar for resistance/resistivity measurements.**

Chambers A and C of the dewar are connected to a turbomolecular pump to hold

a high vacuum. Chamber B is used for liquid nitrogen. Their function is to insulate the inner chamber (D) from the outer environment. The pressure cell, connected to a supporting rod, is inserted in the chamber D, which can be hermetically closed on the top. The temperature is monitored by a diode thermometer inside the cell.

3.1.2 Methods of measurement

The resistance was measured using the 4-contact method. Two leads were connected to the source of constant current, two other leads were connected to the nanovoltmeter. To eliminate the thermal voltage, each data point was calculated from the difference between voltages at direct and reversed polarity of the current source ($V = (V_+ - V_-)/2$, $R = V/I$). Therefore, these techniques together eliminate any contact potentials.

In the quasi-hydrostatic pressure cell the specimen and the lead were connected in series sharing the current leads (Figures 3.5a, 3.6). In the hydrostatic pressure cell the circuits for the Pb strip and specimen were separated (Figures 3.5b, 3.7).[2]

[2]Normally we try to separate the circuits, because we want to pass as little current as possible in order not to influence the transition temperature. Since conductivities of Pb and the specimen might not be the same, the value of the current does not have to be the same. This is possible in the HPC, but the space limitation inside the QHPC makes it difficult. In order to decrease required current, the thickness of the sample and Pb is low.

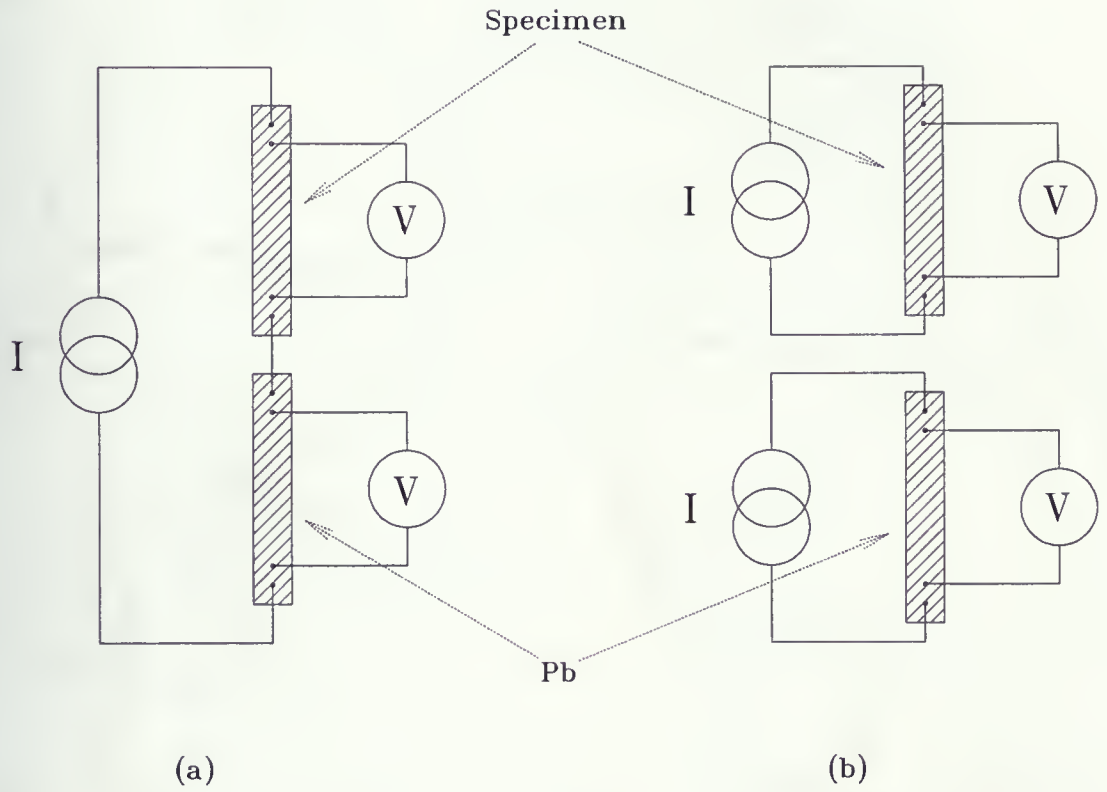

Figure 3.5: **Electrical connections for measurements: (a) QHPC – sample and Pb strip are connected to the source of constant current in series; (b) HPC – sample and lead strip have each their own constant current sources**

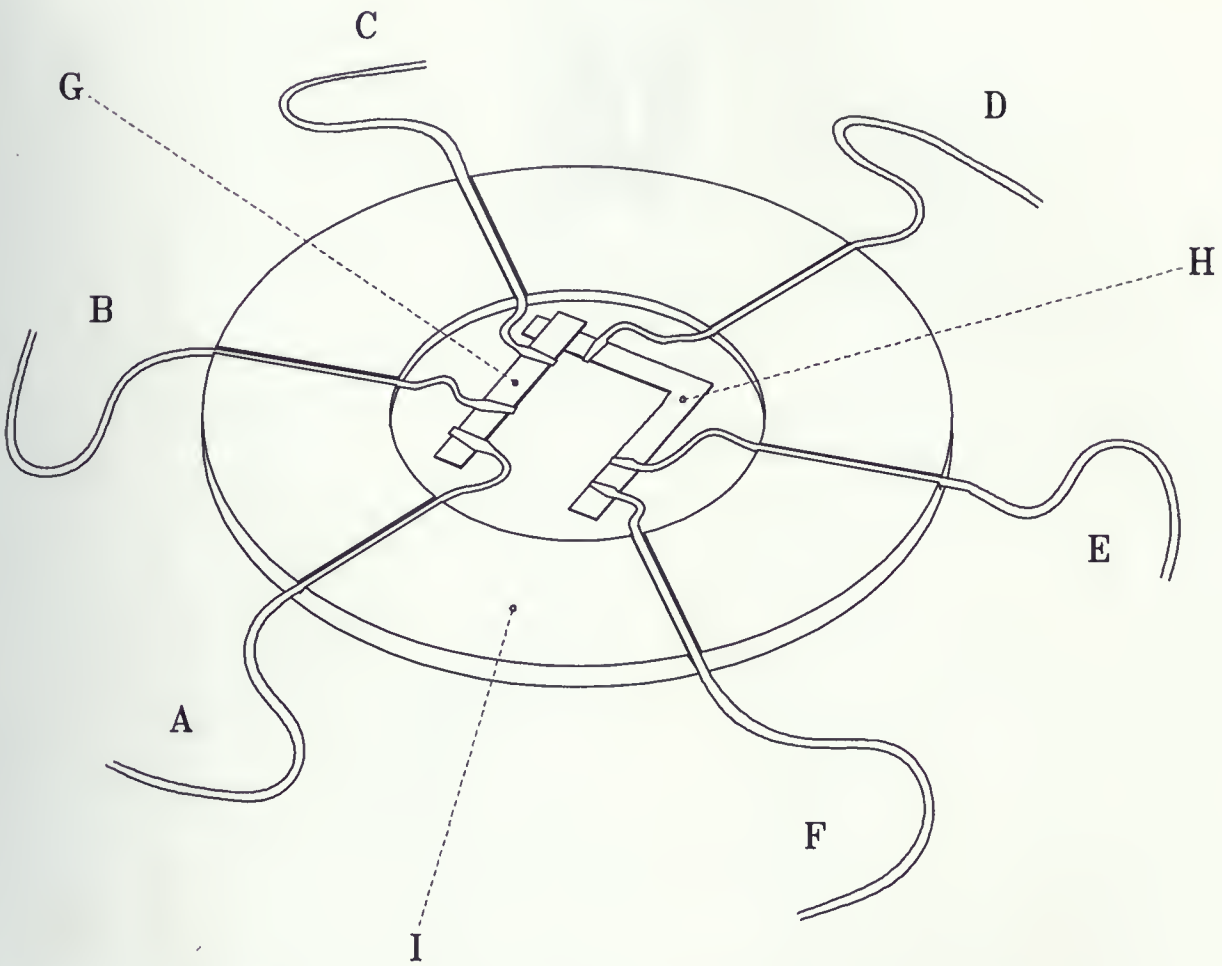

Figure 3.6: **Sample connections inside the quasi-hydrostatic pressure cell (Figure 3.3, part K): A, F – current leads; B, C – voltage leads for MgB_2 sample; D, E – voltage leads for Pb strip; G – MgB_2 sample; H – Pb strip; I – soapstone washer.**

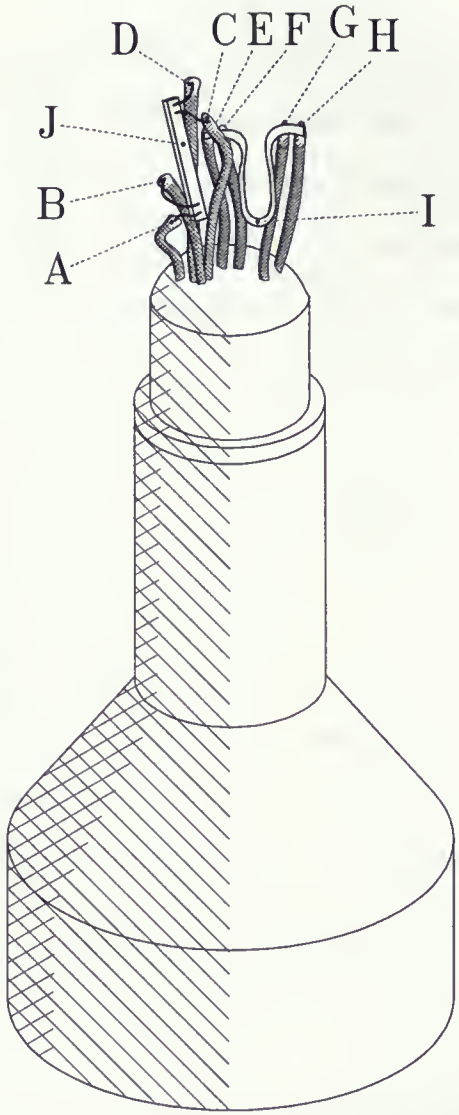

Figure 3.7: **Hydrostatic pressure cell obturator (Figure 3.2, part H) – it shows how specimen and lead ribbon are connected. A, D – current leads for MgB_2; B, C – voltage leads for MgB_2; E, H – current leads for Pb; F, G – voltage leads for Pb; I – Pb ribbon; J – MgB_2 sample.**

3.2 Sample preparation

3.2.1 Fabrication of MgB_2

To fabricate bulk polycrystalline MgB_2, we used the Mg diffusion method. First, we placed the boron powder and magnesium chips in stoichiometric ratios into the tantalum tube and mechanically sealed the tube in argon gas atmosphere ($\sim$ 2 bars, room temperature) by pressing the sides of the tube together (the tantalum tube was already sealed at one end). This mechanical sealing ensures no oxygen leakage while transferring the tube to the next stage: an arc melting device the function of which is to seal the tube by melting the edge of the mechanical seal.

The arc melting device consists of a chamber connected to a diffusion pump. Inside the chamber is a copper holder at the bottom connected to one pole of the power supply and a tungsten tip from the top connected to the other pole. First, we placed the tube (already mechanically sealed) in the holder and closed the chamber. Then, we pumped out the chamber, flushed it twice with argon gas, pumped out again and inflated it with argon to approximately 2 bars. This was necessary to avoid contact between the hot tungsten tip and oxygen. Now we simply welded the tube along the edge from one side to another. To check the quality of the seal, we connected the tube to a mass spectrometer and tried to detect argon molecules. If no argon was detected it means that the tube was sealed properly.

For preventing the reaction of Ta with the air in the furnace, the Ta tube was placed into the quartz tube, which was pumped out and sealed. It was then put into the furnace and heated at 900 °C for two hours. Then the tube was allowed to slowly cool down to room temperature.

3.2.2 Preparation for measurements

Each measurement requires a sample of a certain shape and dimensions. For the measurements with the SQUID magnetometer system, a very small piece of specimen is needed (we used a 0.011 mg sample of MgB_2 and 0.01 mg piece of Pb).

For quasi-hydrostatic measurements, we needed a thin strip with dimensions approximately $0.1 \times 0.05 \times 5$ mm^3 to fit into a pressure cell. First, we used a diamond cutter and then, we continued with sand paper until the desired thickness was reached. An L-shaped Pb ribbon was prepared by rolling a steel cylinder against a piece of glass with lead in between. The desired shape was then carved from a thin Pb layer. The sample and the lead were then placed into the hole on the soapstone washer on the anvil (Figure 3.6). After placing the electrical leads[3], the hole was covered by another soapstone. Then glass fibers were placed on top of electrical leads and glued to insulate electrical leads from the anvil.

The resistivity measurement requires a sample of known dimensions preferably in the shape of a rod where the length is relatively long with respect to its thickness. We decided to cut the sample into a tetragonal bar with a cross-sectional area of 0.44×0.30 mm^2 (Figure 3.8) and a length of approximately 6 mm. The crucial point was to connect gold wires. For this purpose, we used a spot-welding technique. We placed our sample onto a conductive plate connected to one pole of a power supply. The other pole was connected to a sharp piece of graphite. To connect the wire, we placed the wire on the sample surface and touched it with the graphite tip. If the current flowing through the junction was high enough, the gold wire melted to the surface. If it was not, it did not melt at all. If it was too high, however, the wire melted too fast. In both cases we had to adjust the current until we found the right value. After connecting all four wires we measured

[3]The electrical leads had to be carefully placed into grooves in the soapstone washer (Figure 3.6).

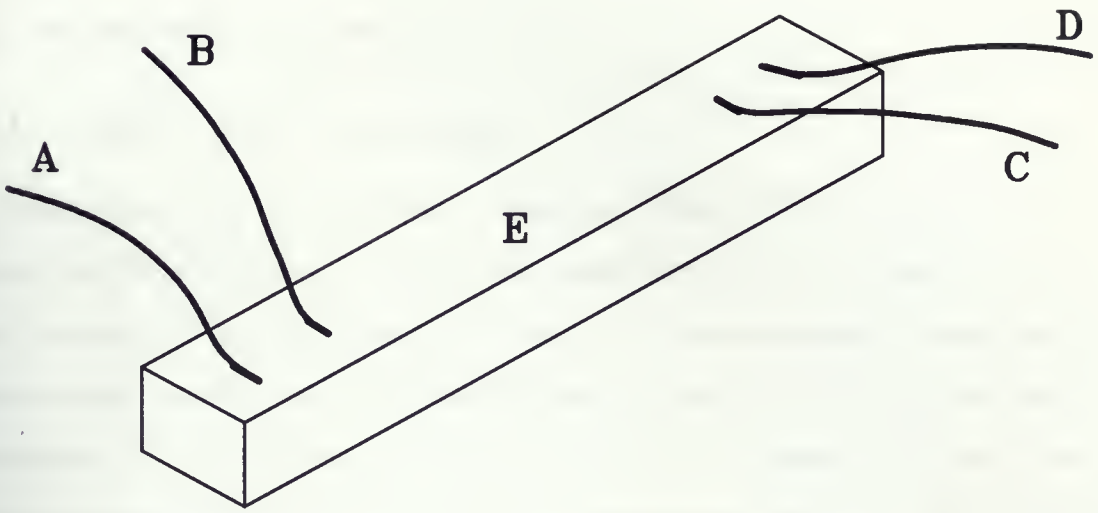

Figure 3.8: **The sample for resistivity measurements: A, B, C, D – Au wires; E – the sample (MgB_2)**

the distance between the wires (their contacts with specimen) B and C (5.34 mm). This is the effective length entering the formula for the calculation of resistivity. The gold wires were then easily connected to the copper wires in the obturator of the pressure cell (Figure 3.7). Another four copper wires of the obturator were connected to a thin Pb ribbon.

3.3 Measurement procedures.

3.3.1 Magnetization measurements

To measure magnetization, we used a Quantum Design SQUID magnetometer. After assembling the pressure cell, we gradually applied force using a hydraulic press before each experiment. For each pressure we performed a measurement of magnetization as a function of temperature. The measurement is controlled by a computer and fully automated. The sample was cooled down to 5 K in zero magnetic field and then, the magnetization was measured as a function of temperature from 5 K to 50 K in a field of 10 Gauss.

3.3.2 Resistance/resistivity measurements

Quasi-hydrostatic pressure

When the cell was assembled, we applied some initial pressure to make a good contact between the electrical leads, the specimen and the lead. This is necessary, because all connections inside the cell are not soldered. After connecting the pressure cell to the system and making sure all contacts are good, the system was ready for measurement.

First we pumped out the vacuum chambers (A and C) of the dewar (Figure 3.4). When the vacuum was high enough ($\sim 10^{-6}$ Torr) we filled the nitrogen chamber (B) with liquid nitrogen. Then, we put the pressure cell into the inner chamber (D), closed it and filled with liquid nitrogen until the temperature dropped down to approximately 80 K. Before transferring liquid helium, we had to transfer *all* liquid nitrogen out of the inner chamber (D). This is very important because if a liquid nitrogen comes into a contact with liquid helium, it freezes and the temperature will never drop down to the temperature of boiling helium (4.2 K). When the inner chamber was empty, we started

to slowly transfer liquid helium until we reached the desired temperature. Then the system was allowed to slowly warm up up to room temperature while the resistance was measured. This procedure was repeated for each applied pressure. Again, the force was applied using a hydraulic press.

Hydrostatic pressure

The measurement with hydrostatic pressure cell was performed on the same system and the same way as the measurement with quasi-hydrostatic pressure cell.

Chapter 4

Results and discussion

4.1 X-ray diffraction

An x-ray diffraction measurement was performed at Max-Planck-Institute, Stuttgart, Germany, to check the purity of the sample. The wavelength of the incident beam was 1.5405 Å (Cu K-alpha line). The results are plotted in Figure 4.1. The pattern is consistent with known crystal structure of MgB_2 (Appendix A). As can be seen, there are some peaks which do not belong to MgB_2. The best candidates for the source of these peaks are MgO, unreacted Mg or B and possibly Ta. To identify them, we compared the pattern with corresponding patterns constructed from data, which were obtained from the x-ray diffraction database [54].

We found data for 5 elemental boron phases, but none of them is present in the specimen.

An important fact is that there is no MgO in our sample. Small amounts of this impurity were reported in other works [5, 28, 40, 41]. This insulator (MgO) would appear as a result of a leakage of oxygen into the tube during the synthesis. Fortunately, the method we used for the sample preparation is appropriate and keeps the tantalum tube well sealed at all times. If found in reasonably small amounts, MgO has no influence on the transition temperature.

Comparing Figures 4.1 and 4.2, we can see that there is some unreacted Mg present in the specimen. A possible reason is that, at the time of synthesizing the sample, some

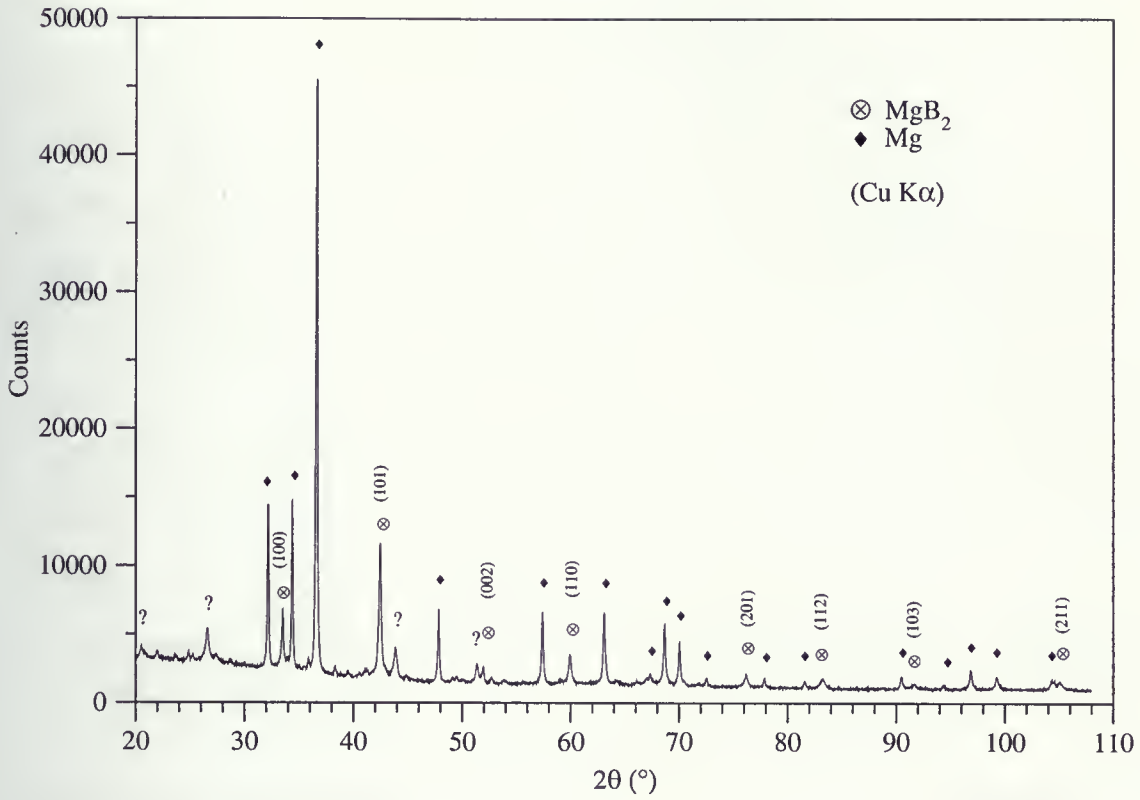

Figure 4.1: **X-ray diffraction pattern of our MgB_2 sample.**

groups recommended to add extra Mg to the initial materials in order to compensate any Mg loss during the synthesis (e.g. Lorenz et al. [41]). This was in the early stages of the research and later it was shown to be unnecessary. But because of this suggestion, we added approximately extra 5wt.% of Mg, therefore the ratio was not stoichiometric. But even considering higher scattering crossection of magnesium, magnesium peaks are still surprisingly high relative to those which belong to MgB_2. Therefore, there might be even higher content of Mg than 5wt.[1] Thus we have a mixture of magnesium and MgB_2 in our

[1]Excess of Mg was reported also by Giunchi [13].

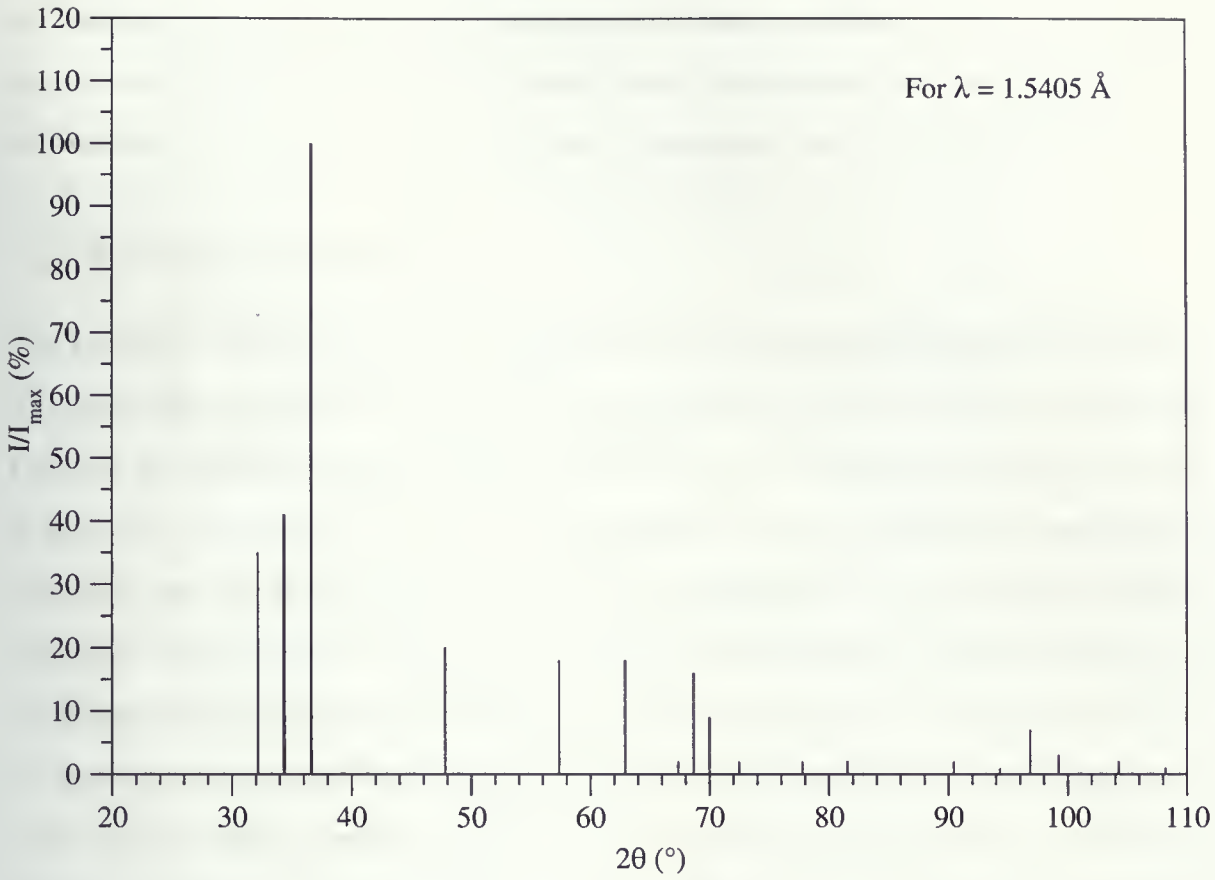

Figure 4.2: **X-ray diffraction pattern of Mg taken from the database [54]**

sample. Excess Mg forms grains of bulk magnesium surrounded by MgB_2. This can be observed in the optical photograph of our sample (Figure 4.10). These grains together with MgB_2 act as sets of parallel and serial resistors with resistivities of MgB_2 and Mg.

Most of the extra peaks belong to magnesium, but there are still some unidentified peaks. The "wetting" effect during synthesis might be a source of traces of tantalum (from the tube), but this is not the case, since the tantalum pattern is not present in our diffraction pattern.[2]Therefore, even if this happened, the amount of Ta was not sufficient to form bulk tantalum structures, which could be seen in the diffraction pattern. It is

[2]We also checked for the presence of Ta_3B_2, TaB, TaB_2, Ta_3B_4, Ta_2B.

not easy to tell what the source of those extra peaks is, we did not find any element known to us having x-ray peaks corresponding to these unidentified peaks. To find out all materials in the specimen, we would have to dissolve it and use plasma spectroscopy.

4.2 Resistivity measurement

The resistivity was calculated from resistance measurement and the sample dimensions. The resistance was measured during a warm up from 4.2 K up to room temperature. Pressure was applied using hydrostatic pressure cell. An example of one measurement is plotted in Figure 4.3. In this set of experiments, we were interested in normal state resistivity near the room temperature. As seen in the Figure 4.4, the resistivity changes only little with pressure. For the sake of comparison each resistivity versus pressure plot for a given temperature was normalized to ambient pressure. Thus enabling each $\rho(P)$ to be placed on one graph (Figure 4.5). In this plot we can see that after an application of pressure the resistivity initially increases and after the pressure reaches a certain point, it starts to decrease. This could be attributed to the fact that the resistivity of metals, as discussed in section 2.3.1, depends mostly on the density of states at the Fermi level ($N(0)$) and the current density of Fermi electrons j_F (ρ is inversely proportional to $N(0)$ and j_F^2). According to calculations of S. Bose [9], the density of states at the Fermi level, in the case of MgB_2, decreases with pressure (Figures 4.7, 4.8). The current density of Fermi electrons increases with pressure, therefore, these quantities "compete". The behavior seen in the Figure 4.5 would indicate that initially $N(0)$ is stronger than j_F^2 and at a certain pressure j_F^2 begins to rise faster than $N(0)$ decreases. This assumes that the contribution of the relaxation time τ is negligible.

Our experimental value of room temperature resistivity is $18 \pm 0.5 \mu\Omega$cm. According to Kong et al. [12] theoretical estimate is about 10 $\mu\Omega$cm. This disagreement is not

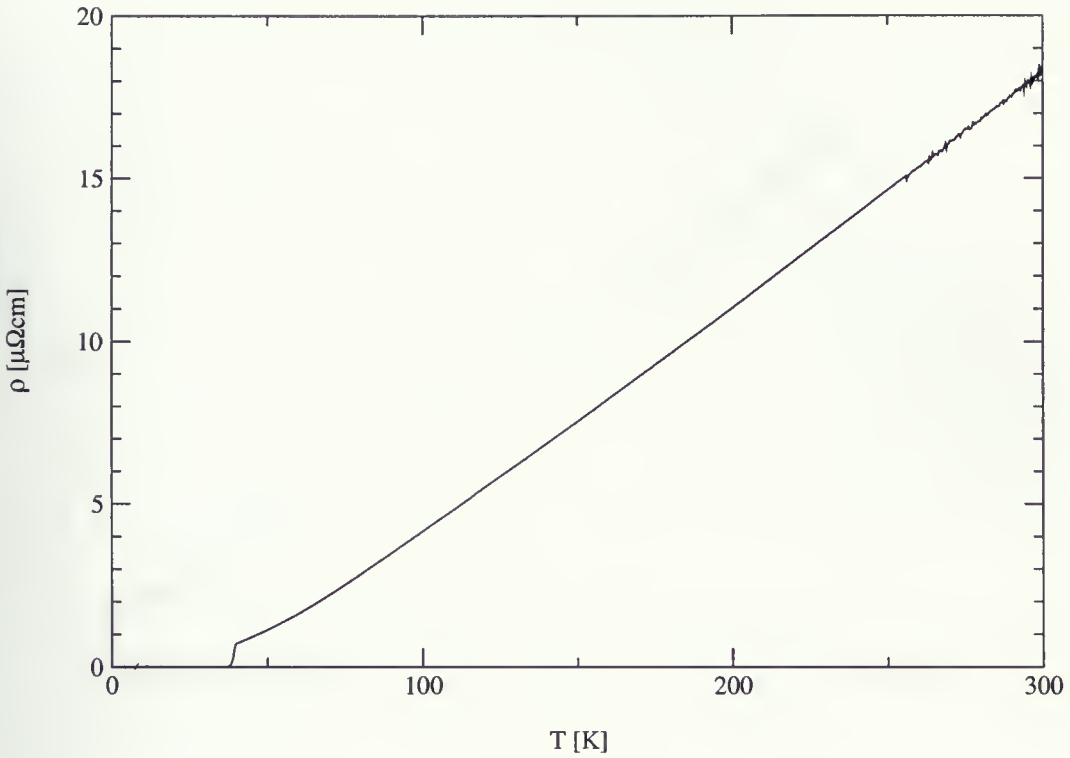

Figure 4.3: **Data from resistivity measurement.** $P = 0.19$ **GPa.**

a problem, however, because theoretical models deal with perfect materials, without impurities, therefore resistivity in real materials is almost always higher. From this point of view the difference is acceptable.

In comparison to other experimental studies (Table 4.1), an obvious discrepancy can be seen. It is necessary to realize that samples were produced by various methods. Up to now, the majority of dense samples were made by high temperature – high pressure (HT-HP) method. Methods using a lower pressure usually produce porous samples [15, 28, 40]. According to Giunchi [13], strains introduced by high pressure remain in the sample even

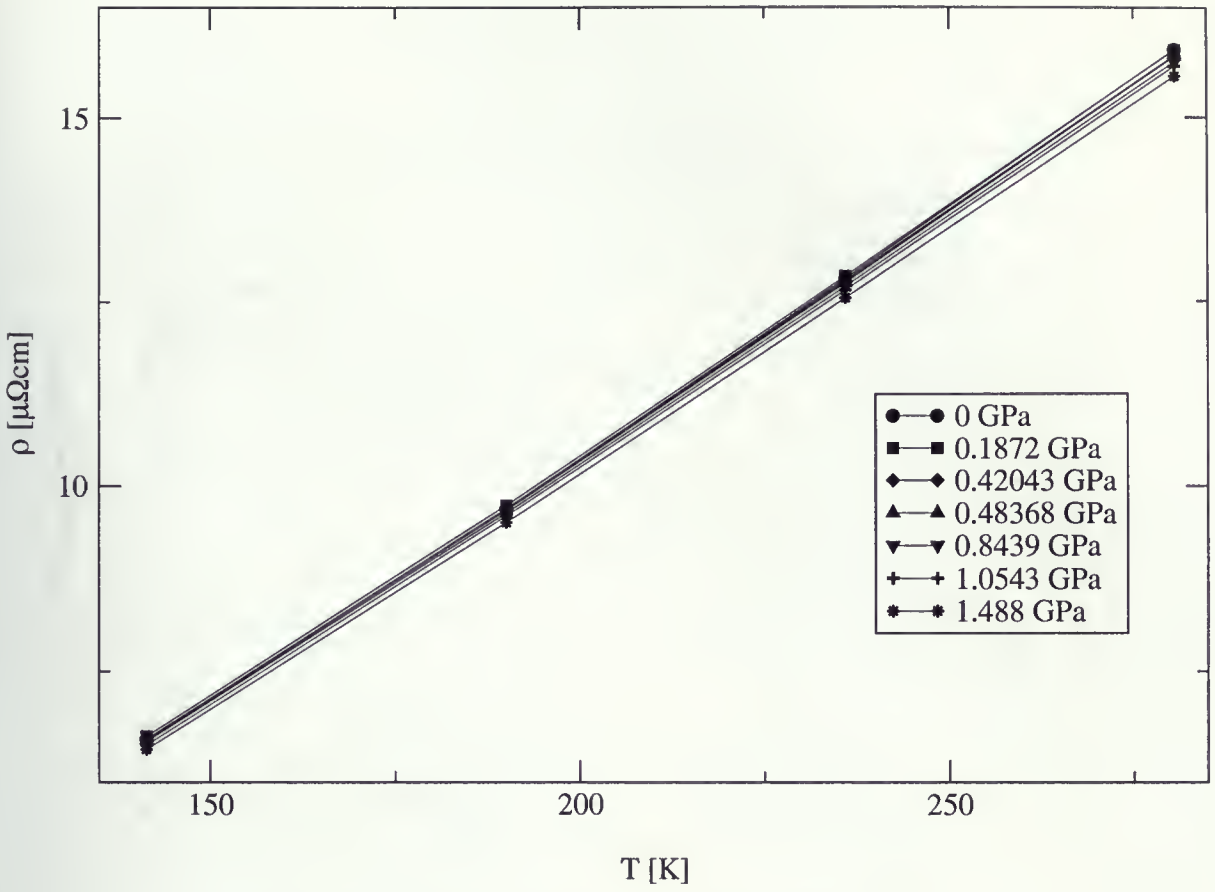

Figure 4.4: **Resistivity of MgB_2 versus temperature.**

after sintering.[3] On the other hand, Deemyad [7] showed that sheer stress has a significant influence on superconducting properties (particularly T_c and dT_c/dP). Therefore, it is reasonable to expect that it has also an influence on normal state resistivity. They report that the largest strains were observed where MgB_4 phase is present as an impurity. We did not find this phase in our specimen.

One would expect that, providing the material is exactly the same, dense samples would appear to have lower resistivity than porous samples, because the resistivity is calculated from the resistance and sample dimensions. So if the material is porous, as

[3]They found a method (reactive liquid Mg infiltration), which produces dense samples without the need of a high pressure apparatus.

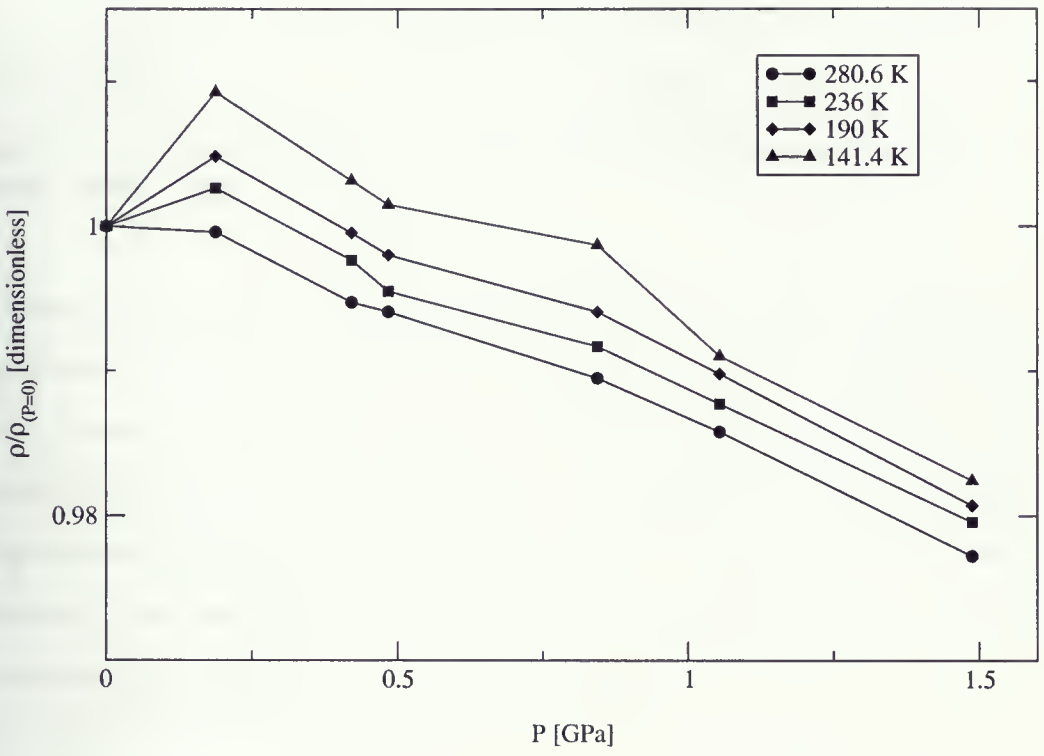

Figure 4.5: **Resistivity of MgB_2 versus hydrostatic pressure.**

reported by those who made samples at lower pressures, the effective cross-sectional area is smaller than the measured one (because the material does not fill the whole space). This causes an error in the calculation, which is then reflected in increased resistivity ($\rho = RA/l$; ρ - resistivity, R - resistance, A - area, l - length).

Another factor is the presence of Mg in the specimen. The resistivity of magnesium is lower than the resistivity of MgB_2 (it is lower than all reported values[4]), that means it decreases the overall resistivity. According to the x-ray powder diffraction pattern

[4]Resistivity of Mg at room temperature is 4.4 $\mu\Omega$cm [53], experimental resistivity of MgB_2 single crystals reported by Lee et al. [42] is 6 $\mu\Omega$cm, which is the lowest reported value

ρ(300K)	Origin	Sample quality	Preparation method
18.4 $\mu\Omega$cm	our measurement	–	conventional
17 $\mu\Omega$cm	Giunchi [13]	dense	react. liq. Mg infiltration
38.2 $\mu\Omega$cm	Schneider [14]	–	conventional
50 $\mu\Omega$cm	Jung [15]	dense	HT-HP

Table 4.1: **Room temperature resistivity of MgB_2 at ambient pressure – experimental values.**

of Giunchi [13], Mg was present in their sample as well. Their sample was synthesized using reactive liquid Mg infiltration, which produces dense samples at lower pressures, which is an advantage in terms of a lack of internal strains. Therefore their resistivity should be even lower than ours, but it is not. This is probably caused by higher content of magnesium in our sample, which can be estimated by comparing our and their diffraction patterns. These results are in agreement with the conclusions of Jung et al. [50] in their research on the effects of unreacted Mg in MgB_2.[5]

4.3 $T_c(P)$ measurements

The transition temperature was measured using two systems: (i) SQUID magnetometer, where we measured dc-magnetization and (ii) resistance/resistivity measurement system. Lead as an internal manometer was used in both cases. For magnetization measurements we used a hydrostatic pressure cell and for resistance measurement a quasi-hydrostatic pressure cell. A quasi-hydrostatic pressure cell allows us to reach higher pressures.

From the temperature dependence of magnetization the transition temperature as a 5% change was determined for each applied pressure. These values (pressure and corresponding T_c) were plotted onto one graph (Figure 4.6a) and the slope (dT_c/dP) was calculated (-1.18 ± 0.05 K/GPa), using linear least squares fit.

[5] E.g. linearity of $\rho(T)$

The same procedure was repeated for quasi-hydrostatic measurements, except that the transition temperature was determined from resistance data by the 50% change (midpoint). The plot T_c versus pressure in this case (Figure 4.6b) yielded $dT_c/dP = -1.2 \pm 0.1$ K/GPa.

4.3.1 Analysis of results

The following discussion is based on the works of Loa and Syassen [2] and Chen et al. [8]. To analyze our $T_c(P)$ data, we employ the McMillan formula [44]:

$$T_c = \frac{\langle\omega_{ln}\rangle}{1.2} \exp\left[-\frac{1.04(1+\lambda)}{\lambda - (1+0.62\lambda)\mu^*}\right] \tag{4.1}$$

where $\langle\omega_{ln}\rangle$ is logarithmically averaged phonon frequency, λ is electron-phonon coupling parameter and μ^* is the Coulomb pseudopotential. In order to find the pressure dependence of this expression we take logarithmic pressure derivative of both sides:

$$\begin{aligned}
\frac{d\ln T_c}{dP} &= \frac{\partial \ln T_c}{\partial \langle\omega_{ln}\rangle}\frac{d\langle\omega_{ln}\rangle}{dP} + \frac{\partial \ln T_c}{\partial\lambda}\frac{d\lambda}{dP} + \frac{\partial \ln T_c}{\partial\mu^*}\frac{d\mu^*}{dP} \\
&= \frac{\partial \ln T_c}{\partial \ln\langle\omega_{ln}\rangle}\frac{d\ln\langle\omega_{ln}\rangle}{dP} + \frac{\partial \ln T_c}{\partial\lambda}\lambda\frac{d\ln\lambda}{dP} + \frac{\partial \ln T_c}{\partial\mu^*}\mu^*\frac{d\ln\mu^*}{dP} \\
&= \frac{d\ln\langle\omega_{ln}\rangle}{dP} + \alpha\frac{d\ln\lambda}{dP} + \beta\frac{d\ln\mu^*}{dP}
\end{aligned} \tag{4.2}$$

where

$$\begin{aligned}
\alpha &\equiv \lambda\frac{\partial \ln T_c}{\partial\lambda} = \frac{1.04\lambda(1+0.38\mu^*)}{(\lambda-\mu^*(1+0.62\lambda))^2} \\
\beta &\equiv \mu^*\frac{\partial \ln T_c}{\partial\mu^*} = -\frac{1.04\mu^*(1+\lambda)(1+0.62\lambda)}{(\lambda-\mu^*(1+0.62\lambda))^2}
\end{aligned} \tag{4.3}$$

Now we know [44]:

$$\lambda = \frac{N(0)\langle I^2\rangle}{M\langle\omega^2\rangle} = \frac{\eta}{M\langle\omega^2\rangle} \tag{4.4}$$

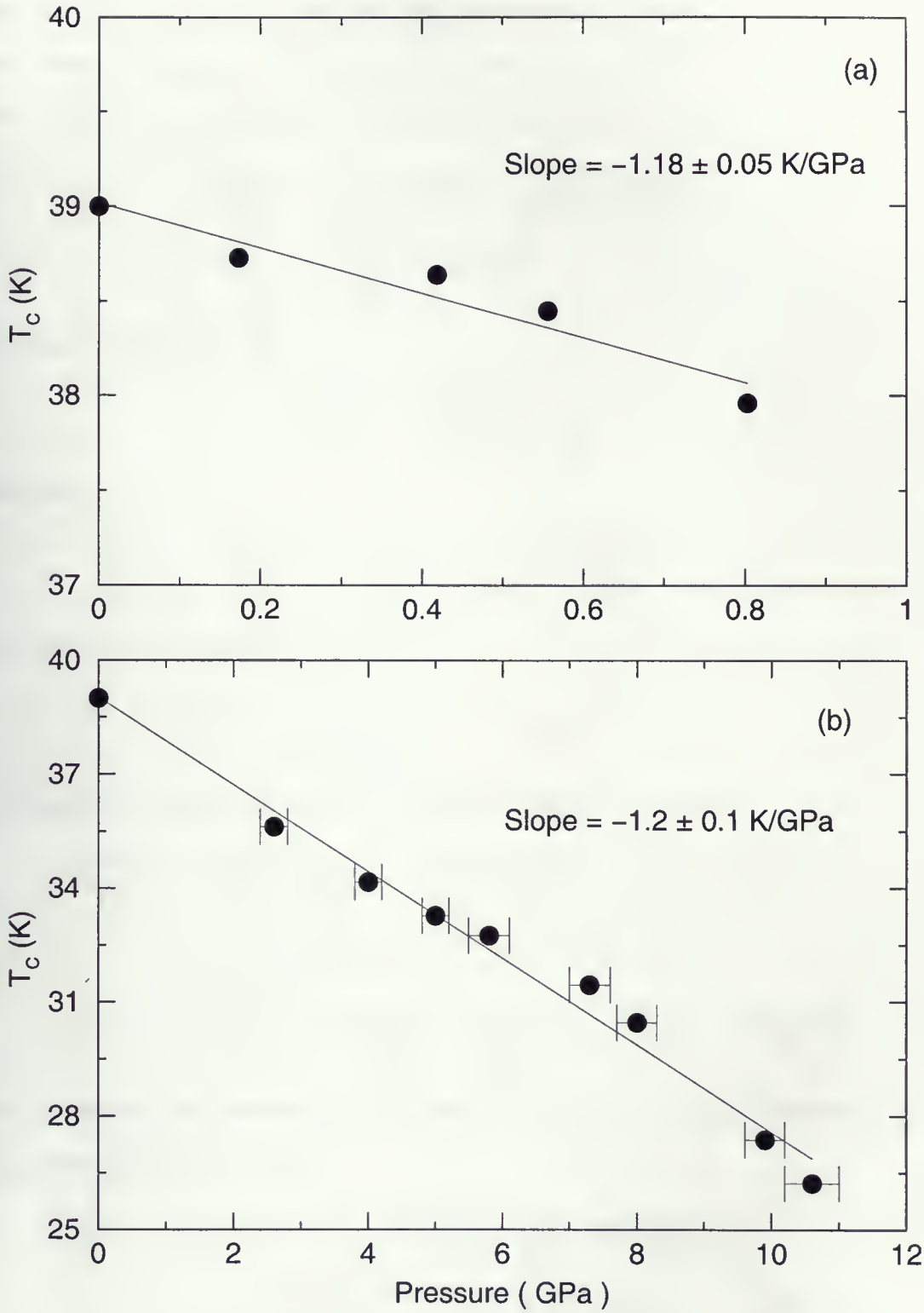

Figure 4.6: **Values of T_c as a function of pressure obtained from (a) magnetization measurements (hydrostatic pressure), (b) resistance measurements (quasi-hydrostatic pressure).**

where $N(0)$ is the density of states at the Fermi level, $\langle I^2 \rangle$ is the averaged electron-ion matrix element squared, M is the atomic mass, η is the McMillan-Hopfield parameter which represents a local "chemical" property of an atom in a crystal. Therefore,

$$\begin{aligned} \frac{d\ln\lambda}{dP} &= \frac{\partial\ln\lambda}{\partial\ln\eta}\frac{d\ln\eta}{dP} + \frac{\partial\ln\lambda}{\partial\ln\langle\omega^2\rangle}\frac{d\ln\langle\omega^2\rangle}{dP} \\ &= \frac{d\ln\eta}{dP} - 2\frac{d\ln\langle\omega\rangle}{dP} \end{aligned} \tag{4.5}$$

According to Chen et al. [8]:

$$\frac{d\ln\eta}{dP} = -\frac{d\ln N(0)}{dP} + \frac{2}{3B} \tag{4.6}$$

which gives

$$\frac{d\ln\lambda}{dP} = -\frac{d\ln N(0)}{dP} + \frac{2}{3B} - 2\frac{d\ln\langle\omega\rangle}{dP} \tag{4.7}$$

where B is the bulk modulus. We use:

$$\mu^* = \frac{\mu}{1+\mu\ln\left(\frac{\omega_p}{\langle\omega\rangle}\right)}, \quad \mu = N(0)V_c\left\langle I^2\right\rangle = \eta V_c \tag{4.8}$$

ω_p is plasma frequency and V_c is the screened Coulomb interaction.

$$\begin{aligned} \frac{d\ln\mu^*}{dP} &= \frac{\partial\ln\mu^*}{\partial\ln\eta}\frac{d\ln\eta}{dP} + \frac{\partial\ln\mu^*}{\partial\ln\omega_p}\frac{d\ln\omega_p}{dP} + \frac{\partial\ln\mu^*}{\partial\ln\langle\omega_{ln}\rangle}\frac{d\ln\langle\omega_{ln}\rangle}{dP} \\ &= \left(\frac{\mu^*}{\mu}\right)\frac{d\ln\eta}{dP} - \mu^*\left(\frac{d\ln\omega_p}{dP} - \frac{d\ln\langle\omega_{ln}\rangle}{dP}\right) \\ &= \left(\frac{\mu^*}{\mu}\right)\left(-\frac{d\ln N(0)}{dP} + \frac{2}{3B}\right) - \mu^*\left(\frac{d\ln\omega_p}{dP} - \frac{d\ln\langle\omega_{ln}\rangle}{dP}\right) \end{aligned} \tag{4.9}$$

From free electron gas estimates we can rewrite $d\ln\omega_p/dP = 1/(2B)$. Substituting these results into equation 4.2 we get:

$$\begin{aligned} \frac{d\ln T_c}{dP} &= \frac{d\ln\langle\omega_{ln}\rangle}{dP} + \alpha\left[-\frac{d\ln N(0)}{dP} + \frac{2}{3B} - 2\frac{d\ln\langle\omega\rangle}{dP}\right] + \\ &\quad + \beta\left[\left(\frac{\mu^*}{\mu}\right)\left(-\frac{d\ln N(0)}{dP} + \frac{2}{3B}\right) - \mu^*\left(\frac{1}{2B} - \frac{d\ln\langle\omega_{ln}\rangle}{dP}\right)\right] = \end{aligned}$$

$$= [1 - 2\alpha + \beta\mu^*] \frac{d \ln \langle\omega\rangle}{dP} + \left[-\alpha - \beta\mu^* \left(\frac{1}{\mu}\right)\right] \frac{d \ln N(0)}{dP} + \\ + \frac{2}{3B}\left[\alpha - \beta\mu^* \left(\frac{3}{4} - \frac{1}{\mu}\right)\right] \tag{4.10}$$

During this derivation we assumed (equations 4.5, 4.10) that

$$\frac{d \ln \langle\omega^2\rangle}{dP} \approx 2\frac{d \ln \langle\omega\rangle}{dP}, \qquad \frac{d \ln \langle\omega_{ln}\rangle}{dP} \approx \frac{d \ln \langle\omega\rangle}{dP} \tag{4.11}$$

This might not be correct and it still has to be verified, but most probably these values of pressure derivatives are very close even if the averages itself are different. However, we make this assumption and if the result of the analysis is acceptable we were probably allowed to do that.

Now we can calculate constants α, β, μ and μ^*. We use the values $\lambda = 0.87$, $\langle\omega_{ln}\rangle = 0.62$ meV (504 cm^{-1}) obtained in the full-potential (FP-LMTO) calculation of Kong et al. [12] and our value T_c =39 K and substitute them into equation 4.1 to obtain μ^*, which yields μ^* =0.1. This value together with ω_p = 7 eV (Kong et al. [12]) is then used in equation 4.8 and $\mu = 0.19$ is obtained. From equations 4.3, we get $\alpha = 1.83$ and $\beta = -0.58$.

At this stage, equation 4.10 consists of pressure derivative of $\ln T_c$ on the left side and three terms on the right side. We have already evaluated constants in each term,but pressure derivatives of phonon frequencies and density of states are still unknown.

The term on the left hand side is a result of our experiments and we found $d \ln T_c/dP \doteq -(1.2/39)$ GPa^{-1} = -3.1% GPa^{-1}.

To evaluate $d \ln N(0)/dP$, we used calculation of the electronic structure of MgB_2 done by S. Bose [9] using the TB-LMTO-ASA program [16]. The density of states calculated for two pressures is plotted in the Figure 4.7. The relationship between pressure and the lattice parameters was obtained from the results of Vogt et al. [3] and Jorgensen et al. [4]. Jorgensen's results are valid for low pressures (up to 0.62 GPa), while Vogt's results are

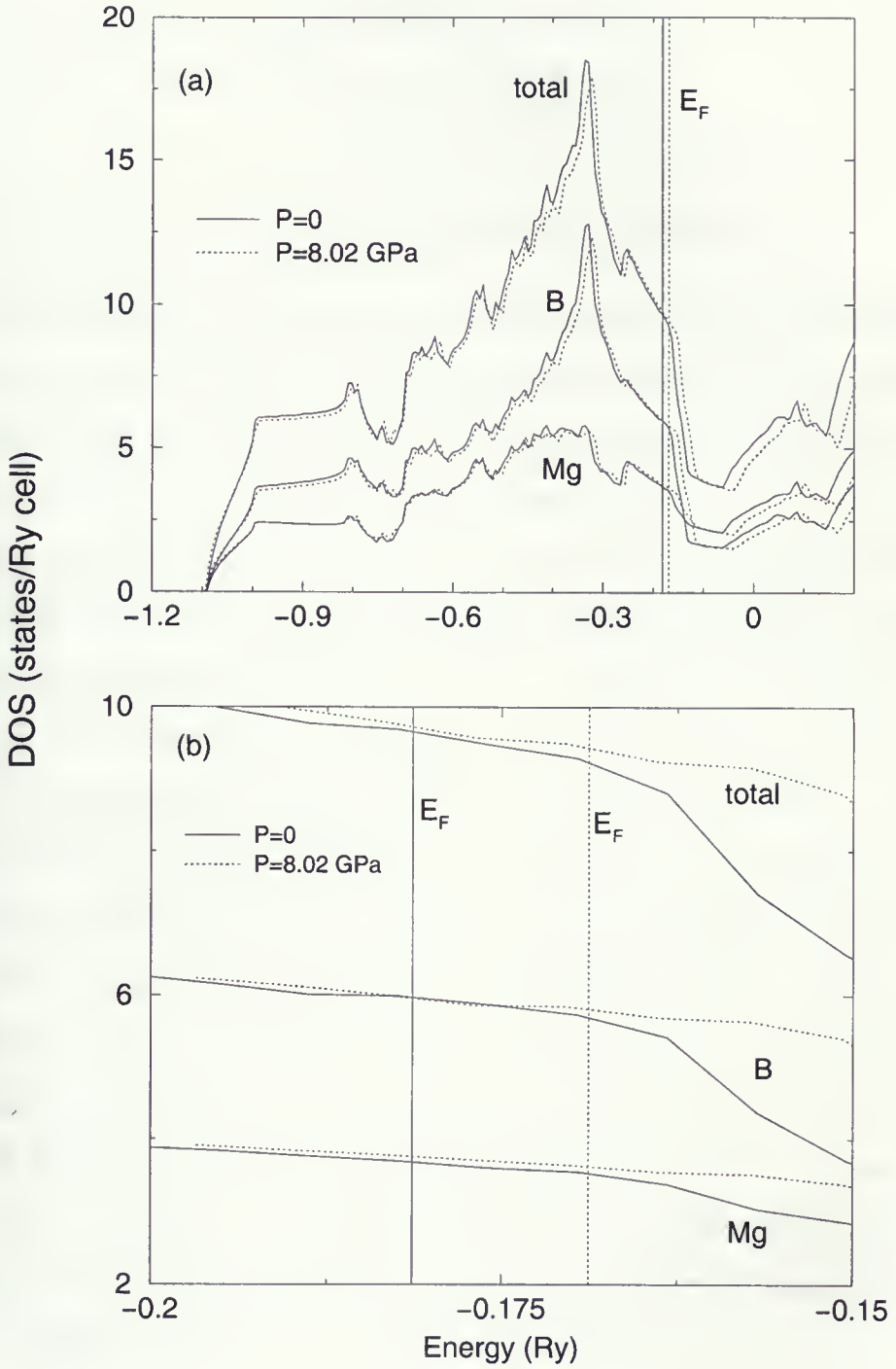

Figure 4.7: **Calculated density of states as a function of energy at 0 and 8 GPa (using pressure-lattice parameter relation from Ref. [3]). Part (b) is magnified view of the region near the Fermi level.**

applicable for high pressures (up to 8.02 GPa). According to Jorgensen et al. [4], lattice parameters a nad c can be expressed as a function of pressure:

$$\begin{aligned} a &= a_0(1 - 0.00187\ \mathrm{GPa}^{-1}P);\ a_0 = 3.0849\ \text{Å} \\ c &= c_0(1 - 0.00307\ \mathrm{GPa}^{-1}P);\ c_0 = 3.5211\ \text{Å} \end{aligned} \tag{4.12}$$

where a_0 and c_0 are lattice parameters at ambient pressure and room temperature, P is the pressure in GPa. This allows us to calculate and plot density of states at Fermi level $N(0)$ for certain values of pressure which is shown in Figure 4.8. From these plots, we calculated $d\ln N(0)/dP$, which can be used in equation 4.10.

As of now we know everything in equation 4.10 except for $d\ln\langle\omega\rangle/dP$, we can solve it for this quantity, which indicates pressure dependance of the average phonon frequency. Depending on which results we use (low pressures of Vogt et al. or high pressures of Jorgensen et al.), we obtain two values of $d\ln N(0)/dP$. The results and all quantities used in our calculation are summarized in Table 4.2. Thus by using pressure-lattice relations of Vogt, we obtained $d\ln\langle\omega\rangle/dP = 1.6\,\%\ \mathrm{GPa}^{-1}$, using Jorgensen's results we obtained the same value $d\ln\langle\omega\rangle/dP = 1.6\,\%\ \mathrm{GPa}^{-1}$. This is a measure of how much the pressure affects the average phonon frequency. For comparison, the pressure dependence of the density of states at Fermi level is only $-0.29\ \%\ \mathrm{GPa}^{-1}$ ($-0.33\ \%\ \mathrm{GPa}^{-1}$). For establishing the real influence on the change of the transition temperature, we have to realize that the quantities ($d\ln\langle\omega\rangle/dP$, $d\ln N(0)/dP$) in equation 4.10 are weighted by some factors. Therefore, their real contribution to the total change of transition temperature due to pressure also depends on these factors. Now, if we use results of the calculation (numerical values), the equation 4.10 becomes:

$$\frac{d\ln T_c}{dP} = -2.7\frac{d\ln\langle\omega\rangle}{dP} - 1.5\frac{d\ln N(0)}{dP} + 0.70\%$$

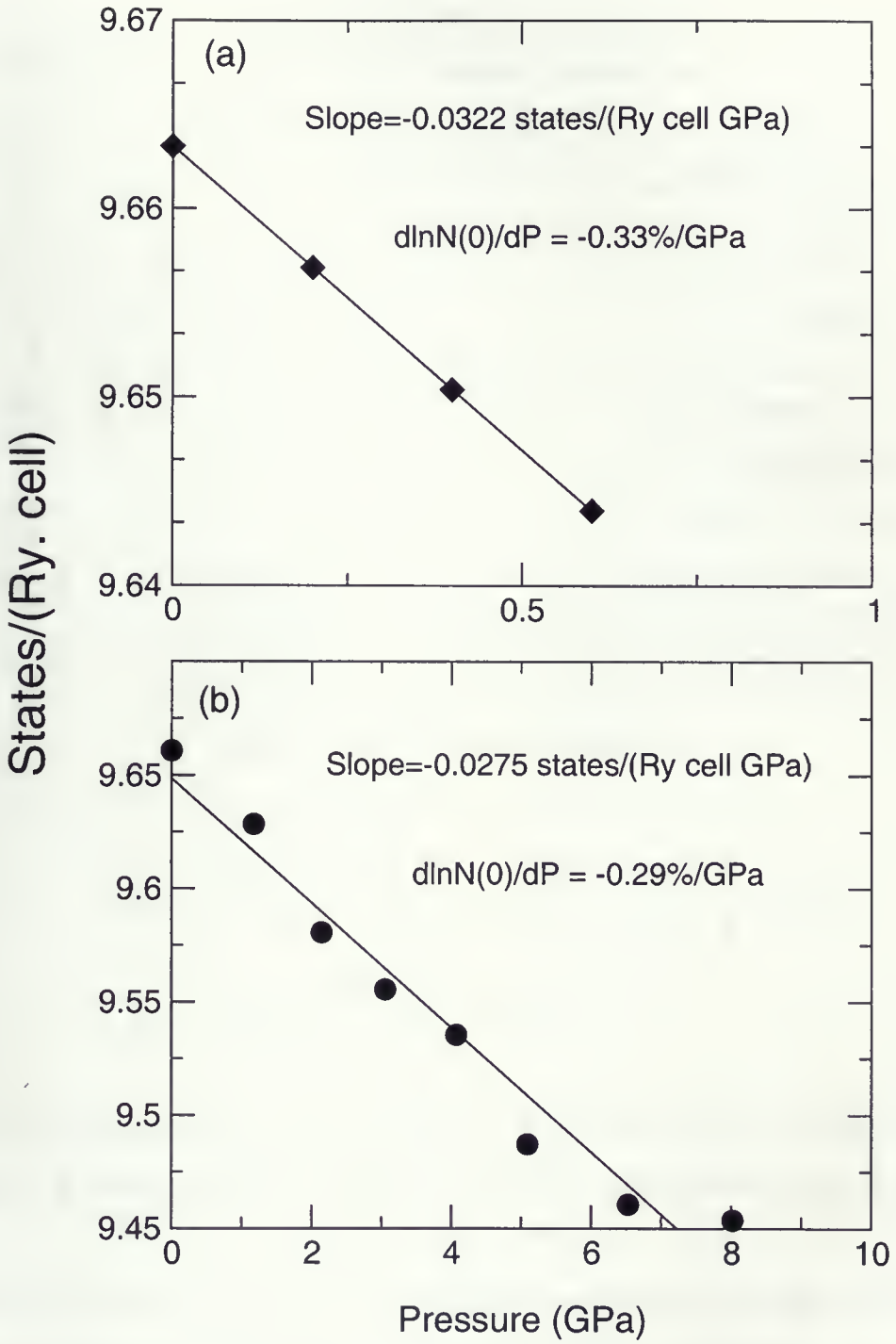

Figure 4.8: **Density of states in MgB_2 as a function of pressure, calculated via LMTO method: (a) pressure-lattice parameter relation from Ref. [4], (b) pressure-lattice parameter relation from Ref. [3].**

quantity	value	origin
λ	0.87	
$\langle\omega_{ln}\rangle$	0.62 meV	Kong [12]
T_c	39 K	experimental value
μ^*	0.1	calculated
ω_p	7 eV	Kong [12]
μ	0.19	
α	1.8	calculated
β	-0.58	
$\frac{d\ln T_c}{dP}$	-3.1 % GPa^{-1}	our experimental value
B	150 GPa	Vogt et al. [3]
$\frac{d\ln\omega_p}{dP}$	0.33 % GPa^{-1}	free electron gas estimate
$\frac{d\ln N(0)}{dP}$	-0.29 % GPa^{-1}	calculated (using Vogt's results)
	-0.33 % GPa^{-1}	calculated (using Jorgensen's results)
$\frac{d\ln\langle\omega\rangle}{dP}$	1.6 % GPa^{-1}	calculated (using Vogt's results)
	1.6 % GPa^{-1}	calculated (using Jorgensen's results)

Table 4.2: **Results of calculations.**

$$
\begin{aligned}
&= -2.7 \times \left\{ \begin{array}{c} 1.6\% \\ 1.6\% \end{array} \right\} - 1.5 \times \left\{ \begin{array}{c} (-0.29\%) \\ (-0.33\%) \end{array} \right\} + 0.70\% \\
&= -4.3\% + \left\{ \begin{array}{c} 0.43\% \\ 0.50\% \end{array} \right\} + 0.70\% \qquad (4.13)
\end{aligned}
$$

where the top value in curly brackets represents the result obtained by using the lattice parameters - pressure dependence by Vogt et al. [3], the bottom value is by Jorgensen et al [4].

From this we can see, that 79% (78%) of the total change of T_c (this number corresponds to the value of -4.3 relative to the other values in the equation 4.13; here the contribution of all of them is meant to be 100%) is caused by the change of phonon frequencies, whereas the contribution of the density of states at the Fermi level is only

8.2% (9.2%).

One modification that can be made in our derivation, however, is to use

$$\frac{d\ln\mu^*}{dP} = \mu^*\left[\frac{d\ln\langle\omega\rangle}{dP} + \frac{1-e^{-2\mu}}{2\mu^2}\left(-\frac{d\ln N(0)}{dP} + \frac{2}{3B}\right) - \frac{2}{3B}\right] \tag{4.14}$$

derived by Chen et al. [8]. Equation 4.10 then becomes:

$$\begin{aligned}\frac{d\ln T_c}{dP} &= [1-2\alpha+\beta\mu^*]\frac{d\ln\langle\omega\rangle}{dP} + \left[-\alpha-\beta\mu^*\frac{1-e^{-2\mu}}{2\mu^2}\right]\frac{d\ln N(0)}{dP} + \\ &+ \frac{2}{3B}\left[\alpha-\beta\mu^*\left(1-\frac{1-e^{-2\mu}}{2\mu^2}\right)\right]\end{aligned} \tag{4.15}$$

This leads then to $d\ln\langle\omega\rangle/dP = 1.6\%$ (1.6%), which is the same as the result of the first calculation. The equation 4.13 is now:

$$\begin{aligned}\frac{d\ln T_c}{dP} &= -2.7\times 1.6\% - 1.6\times\left\{\begin{array}{c}(-0.29\%)\\(-0.33\%)\end{array}\right\} + 0.73\% \\ &= \left\{\begin{array}{c}-4.3\%\\-4.4\%\end{array}\right\} + \left\{\begin{array}{c}0.46\%\\0.52\%\end{array}\right\} + 0.73\%\end{aligned} \tag{4.16}$$

In this case the contribution by phonon frequencies is 78% and the density of states at the Fermi level is 8.3% (9.5%). The last term in both cases is proportional to $1/B$, which, by definition of bulk modulus, is compressibility of the specimen. Note that this is an explicit dependence, because bulk modulus is dependent on the density of states; all terms in equations 4.13 and 4.16 are related.

In both cases, the dominant influence on the value of T_c is the variation of phonon frequencies.

From the value of $d\ln\langle\omega\rangle/dP$ we can calculate the Grüneisen parameter:

$$\gamma_G = \frac{d\ln\langle\omega\rangle}{dP}B = 2.4 \tag{4.17}$$

which turns out to be almost the same whether using Jorgensen's or Vogt's results. This is very close to the results of Deemyad (2.36 and 2.39) [7], Raman spectroscopy measurements of Goncharov et al. (2.9) [35], *ab initio* calculations of Roundy et al. (2.3) [36].

Somewhat lower values were reported by Chen et al. (1.2 calculated using Grüneisen equation and 1.83 obtained from Slater approximation) [8].

The value of dT_c/dP obtained from our experiments (-1.2 ± 0.05 K/GPa) lies within the range of results of another experimental studies: -1.11 K/GPa [7], -1.2 K/GPa [37], -1.45 K/GPa [41], -1.6 K/GPa [40], -2.0 K/GPa [38], [39]. Calculated values include: -0.78 K/GPa and -1.12 K/GPa [8] and -1.8 K/GPa [11].

It is interesting that we obtained very similar pressure derivative of T_c from both techniques we used (i.e. hydrostatic and quasi-hydrostatic). This would suggest that the method of measurement and pressure transmitting medium play little role in terms of the value of dT_c/dP. But Deemyad et al. [7] report that, according to their experimental study, nonhydrostatic pressure transmitting medium introduces shear stress that causes plastic deformations. These deformations have an influence on superconducting properties. They showed that this effect is more significant than differences among the samples and their stoichiometry, which was the earlier explanation of this behavior [41].[6] The best value for pressure derivative of the transition temperature, obtained at purely hydrostatic conditions by Deemyad et al.[7], is -1.11 K/GPa. Thus we probably managed to secure nearly hydrostatic conditions, even though we did not use the He-gas transmitting medium.

As shown in section 2.3.2, it is possible to derive expression for T_c as an explicit function of pressure. Until now we assumed that $\langle\omega_{ln}\rangle$, μ^* and λ are constant with respect to pressure. Now we let them be functions of pressure and substitute them into McMillan formula:

$$T_c = \frac{\langle\omega_{ln}\rangle(P)}{1.2} \exp\left[-\frac{1.04(1+\lambda(P))}{\lambda(P) - (1+0.62\lambda(P))\mu^*(P)}\right] \tag{4.18}$$

[6] They (Deemyad et.al) ran measurements with different pressure media on the same sample.

where

$$\langle\omega_{ln}\rangle(P) = \langle\omega_{ln}\rangle(0)\left(1+\frac{B'}{B}P\right)^{\frac{B}{B'}\frac{d\langle\omega_{ln}\rangle}{dP}} \tag{4.19}$$

$$\lambda(P) = \lambda(0)\left(1+\frac{B'}{B}P\right)^{\frac{B}{B'}\frac{d\ln\lambda}{dP}} \tag{4.20}$$

$$\mu^*(P) = \mu^*(0)\left(1+\frac{B'}{B}P\right)^{\frac{B}{B'}\frac{d\ln\mu^*}{dP}} \tag{4.21}$$

Value of B' can be obtained for example from the Table 1 of reference [11], the rest of all quantities can be calculated from results of this analysis. All values are listed in Table 4.3.

Using these values, the function can be plotted and compared with our experimental data (Figure 4.9). The agreement is very good and indicates that the behaviour of MgB_2 under pressure can be well described by using the McMillan formula. This, in turn, suggests that MgB_2 is a conventional BCS superconductor.

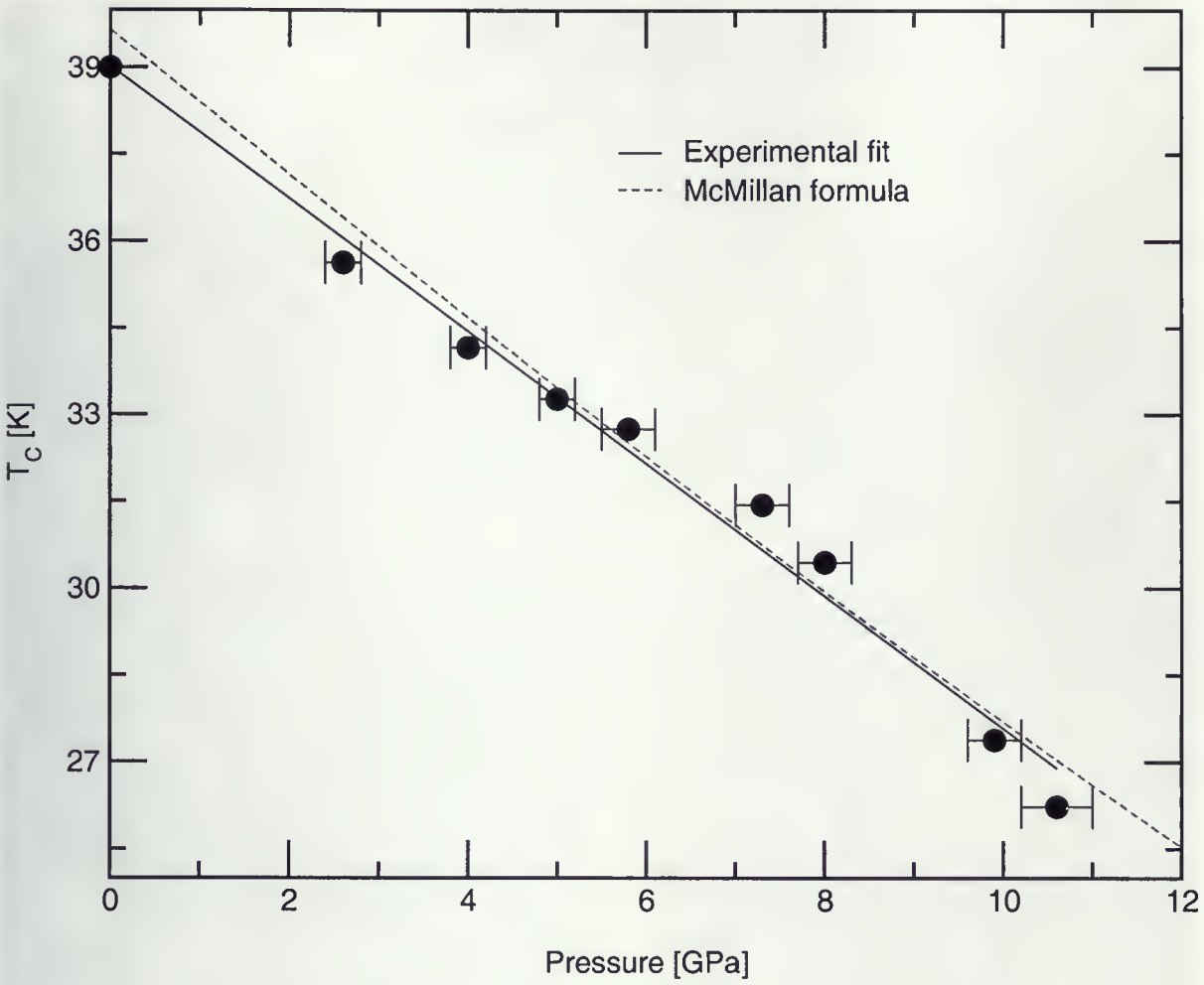

Figure 4.9: **Pressure dependent McMillan formula is plotted and compared with our experimental data.**

$\langle\omega_{ln}\rangle(0)$	719.5 K (0.62 meV)
$\lambda(0)$	0.87 [12]
$\mu^*(0)$	0.1
$d\ln\langle\omega\rangle/dP$	0.016 GPa^{-1}
$d\ln\lambda/dP$	-0.025 GPa^{-1}
$d\ln\mu^*/dP$	0.0052 GPa^{-1}
B	150 GPa [3]
B'	4 [11]

Table 4.3: **Values of quantities used in equations 4.18–4.21.**

Figure 4.10: **Polished surface of MgB_2 sample.**

Chapter 5

Conclusions

In this experimental study we prepared bulk samples of the new superconductor MgB_2 and measured the pressure dependence of the transition temperature and the resistivity. We made attempts to substitute elements but all of them were unsuccessful. This was probably bacause only a few elements substitute for Mg or B [26, 27, 28, 29, 30, 31, 32, 33, 34, 48]. High hopes were put into Na doping because, according to theoretical predictions [24], this was a good candidate to increase the transition temperature. However, there are obvious difficulties in preparation such samples because of the high sodium volatility and difficulty in handling.

We measured the transition temperature as a function of pressure, using two techniques. We obtained similar pressure derivatives of the T_c with both techniques: hydrostatic pressure magnetization measurements yielded -1.18 ± 0.05 K/GPa and quasi-hydrostatic pressure resistivity measurements yielded -1.2 ± 0.1 K/GPa. This agreement however, is only coincidence or perhaps it is that the pressure inside the quasi-hydrostatic pressure cell was distributed nearly uniformly and similar to the hydrostatic pressure.

dT_c/dP was then used in the theoretical model and we concluded that the main contribution to the change of the transition temperature with pressure is due to the changes in the phonon frequencies. The Grüneisen parameter was calculated ($\gamma_G = 2.4$) and found to be within experimental error of other published values [7, 35, 36].

From the above we concluded that magnesium di-boride is a conventional superconductor. It has an extraordinarily high transition temperature that is in contrast to its

simple binary AlB_2-type metallic structure.

Appendix A

Crystal structure of MgB_2

The lattice structure of MgB_2 is a simple hexagonal unit cell with a 3-atom basis (Figure A.1). It contains graphite-type boron layers that are separated by hexagonally close-packed layers of magnesium. Primitive translation vectors are $\vec{a} = a(1, 0, 0)$, $\vec{b} = a(1/2, \sqrt{3}/2, 0)$, $\vec{c} = c(0, 0, 1)$. The position of magnesium atom is (0, 0, 0), positions of boron atoms are (1/3, 1/3, 1/2) and (2/3, 2/3, 1/2).

The distance between boron layers is much larger than interatomic distances within the plane. Also the response to pressure shows that the bonds between planes are weaker than interplanar bonds [4]. The c/a ratio decreases with pressure. The compressibility is 64% larger along the c axis than it is along the ab plane [4].

The lattice parameters at room temperature and ambient pressure are:

$$a_0 = 3.0849 \text{ Å}$$

$$c_0 = 3.5211 \text{ Å}$$

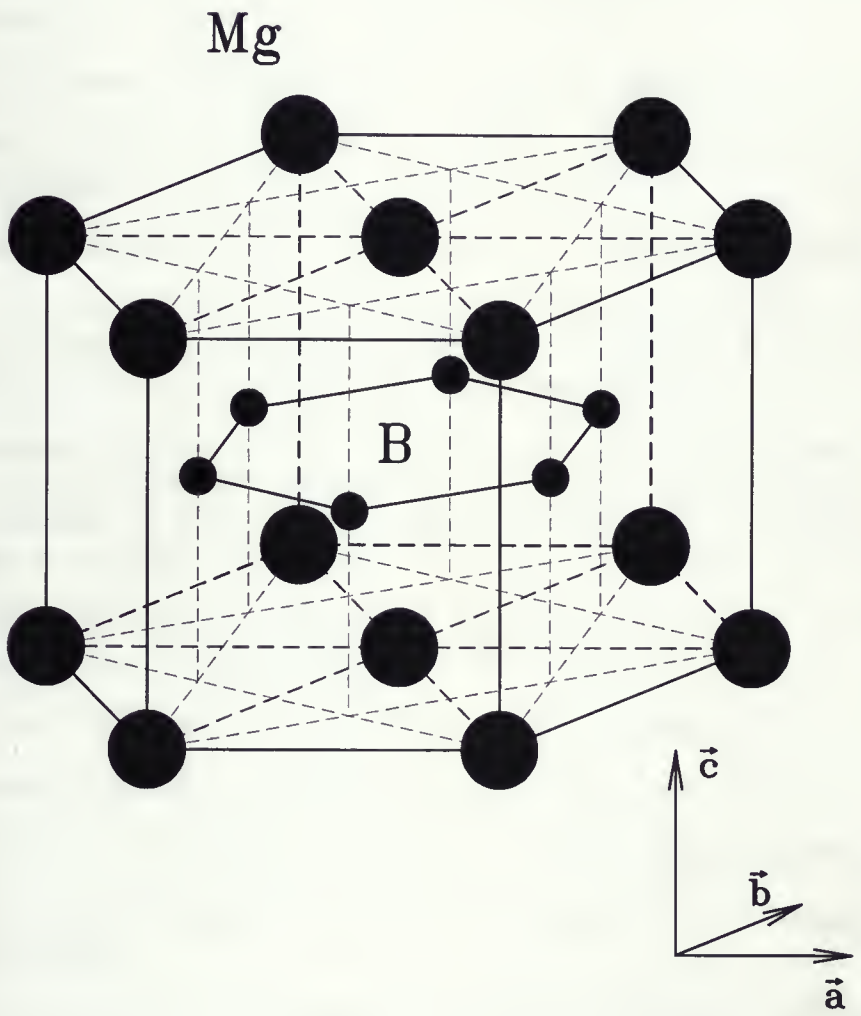

Figure A.1: **MgB_2 lattice.**

Bibliography

[1] J. Akimitsu, Symposium on Transition Metal Oxides, Sendai, January 2001; J. Nagamatsu et al., Nature **410**, 63 (2001).

[2] I. Loa, K. Syassen, Solid State Comm. **118**, 279-282 (2001).

[3] T. Vogt, G. Schneider, J. A. Hriljac, G. Yang, J. S. Abell, Phys. Rev. B **63**, 220505(R) (2001).

[4] J. D. Jorgensen, D. G. Hinks, S. Short, Phys. Rev. B **63**, 224522 (2001).

[5] V. N. Narozhnyi, G. Fuchs, A. Handstein, A. Gümbel, J. Eckert, K. Nenkov, D. Hinz, O. Gutfleisch, A. Wälte, L. N. Bogacheva, I. E. Kostyleva, K.-H. Müller, L. Schultz, preprint: http://arXiv.org/abs/cond-mat/0206513

[6] D. C. Larbalestier, L. D. Cooley, M. O. Rikel, A. A. Polyanskii, J. Jiang, S. Patnaik, X. Y. Cai, D. M. Feldman, A. Gurevich, A. A. Squitieri, M. T. Naus, C. B. Eom, E. E. Hellstorm, R. J. Cava, K. A. Regan, N. Rogadao, M. A. Hayward, T. He, J. S. Slusky, P. Khalifah, K. Inumaru and M. Haas, *Nature* **410**, 186 (2001)

[7] S. Deemyad, T. Tomita, J.J. Hamlin, B.R. Beckett, J.S. Schilling, D.G. Hinks, J.D. Jorgernsen, S. Lee, S. Tajima, Physica C **385**, 105 (2003)

[8] X. J. Chen, H. Zhang, H.-U. Habermeier, Phys. Rev. B **65** (2002).

[9] F. S. Razavi, S. K. Bose, H. Ploczek, Physica C **366**, 73-79 (2002).

[10] Ch. Buzea, T. Yamashita, Superconductor, Science & Technology, 2001.

[11] K. Kunc, I. Loa, K. Syassen, R. K Kremer, K. Ahn, J. Phys.: Condens. Matter **13**, 9945–9962 (2001)

[12] Y. Kong, O.V. Dolgov. O.Jepsen, O.K. Andersen, Phys. Rev. B **64**, 020501(R) (2001).

[13] Giovanni Giunchi, preprint: http://arXiv.org/abs/cond-mat/0208040

[14] M. Schneider, D. Lipp, A. Gladun, P. Zahn, A. Handstein, G. Fuchs, S.-L. Drechsler, M. Richter, K.-H. Müller and H. Rosner, Physica C **363**, 6 (2001).

[15] C. U. Jung, M.-S. Park, W. N. Kang, M.-S. Kim, S. Y. Lee and S.-I. Lee, Physica C **353**, 162 (2001).

[16] Stuttgart TB-LMTO-ASA program, LMTO46, www.fkf.mpg.de/andersen/.

[17] S. L. Budko, C. Petrovic, G. Lapertot, C. E. Cunningham, P. C. Canfield, M.-H. Jung, A. H. Lacerda, Phys. Rev. B **63**, 220503 (2001).

[18] D. G. Hinks, H. Claus, J. D. Jorgensen, Nature **411**, 457 (2001).

[19] S. L. Bud'ko, G. Lapertot, C Petrovic, C. E. Cunningham, N. Anderson, P. C. Canfield, Phys. Rev. Lett **86**, 1877 (2001).

[20] A. V. Pronin, A. Pimenov, A Loidl, S. I. Krasnosvobodstev, Phys. Rev. Lett. **87**, 097003 (2001).

[21] C. Panagopoulos, B. D. Rainford, T. Xiang, C. A. Scott, M. Kambara, I. Inoue, Physical Review B vol **64**, 094514 (2001)

[22] N. Klein, B. B. Jin, J. Schubert, M. Schuster, H. R. Yi, A. Pimenov, A. Loidl, S. I. Krasnosvobodstev, preprint: cond-mat/0107259 (2001).

[23] R. Jin, M. Paranthaman, H. Y. Zhai, H. M. Christen, D. K. Christen, D. Mandrus, preprint: http://arXiv.org/abs/cond-mat/cond-mat/0104411 (2001).

[24] L. M. Volkova, S. A. Polyshchuk, S. A. Magarill, F. E. Herbeck, preprint: http://arXiv.org/abs/cond-mat/cond-mat/0108295

[25] T. Yildirim, Materials Today, p40, April (2002)

[26] R.A. Ribeiro, S.L. Bud'ko, C. Petrovic, P.C. Canfield, preprint: http://arXiv.org/abs/cond-mat/0210530

[27] Y. G. Zhao, X. P. Zhang, P. T Qiao, H. T. Zhang, S. L. Jia. B. S. Cao, M. H. Zhu, Z. H. Han, X. L. Wang, B. L. Gu, Physica C **361**, 91-94 (2001)

[28] P. Toulemonde, N. Musolino, H. L. Suo and R. Flükiger, preprint: http://arXiv.org/abs/cond-mat/0206409

[29] M. Paranthaman, J.R. Thompson, and D.K. Christen, Physica C, **355**, 1 (2001).

[30] J. S. Ahn, and E. J. Choi, preprint: http://arXiv.org/abs/cond-mat/0103169.

[31] T. Takenobu, T. Ito, Dam Hieu Chi, K. Prassides, and Y. Iwasa, Phys. Rev. B **64**, 134513 (2001).

[32] W. Mickelson, J. Cumings, W. Q. Han, and A. Zettl, Phys. Rev. B **65**, 052505 (2002).

[33] Zhao-hua Cheng, Bao-gen Shen, Jian Zhang, Shao-ying Zhang, Tong-yun Zhao, and Hong-wu Zhao, J. Appl. Phys. **91**, 7125 (2002).

[34] A. Bharathi, S. Jemina Balaselvi, S. Kalavathi, G. L. N. Reddy, V. Sankara Sastry, Y. Hariharan, and T. S. Radhakrishnan, Physica C **370**, 211 (2002).

[35] A. F. Goncharov, V. V. Struzhkin, E. Gregoryanz, J. Hu, R. J. Hemley, H.-K. Mao, G. Lapertot, S. L. Bun'ko, and P. C. Canfield, Phys. Rev. B **64**, 100509 (2001).

[36] D. Roundy, H. J. Choi, H. Sun, S. G. Louie, and M. L. Cohen (unpublished).

[37] S. Deemyad, J. S. Schilling, V. G. Tissen, N. N. Koleshnikov, M. P. Kulakov (unpublished).

[38] V. G. Tissen, M. V. Nefedova, N. N. Koleshnikov, M. P. Kulakov, Physica C **363**, 194 (2001).

[39] T. Masui, K. Yoshida, S. Lee, A. Yamamoto, S. Tajima, Phys. Rev. B **65**, 214513 (2002).

[40] B. Lorenz, R. L. Meng, and C. W. Chu, Phys. Rev. B **64**, 12507 (2001).

[41] B. Lorenz, R. L. Meng, and C. W. Chu, preprint: http://arXiv.org/abs/cond-mat/0104303 (2001).

[42] S.Lee, H.Mori, T.Masui, Yu.Eltsev, A.Yamamoto, S.Tajima, J. Phys. Soc. Jpn. **70**, pp.2255-2258 (2001)

[43] W. L. McMillan, Phys. Rev **167**, 331 (1968).

[44] P. B. Allen, Phys. Rev. B **12**, (1975).

[45] G. M. Eliashberg, Zh. Eksp. Teor. Fiz. **38**, 966 (1960); **39**, 1437 (1960) [Sov. Phys.-JETP **11**, 696 (1960); **12**, 1000 (1961)].

[46] M. Tinkham, G. McKay, *Introduction to superconductivity*, (New York: McGraw-Hill, Inc., 1996).

[47] R. D. Parks, *Supercoductivity*, (New York: Marcel Dekker, Inc., 1969).

[48] J. S. Slusky, N. Rogado, K. W. Reagan, M. A. Hayward, P. Hkalifah. T. He, K. Inumaru, S. Loureiro, M. K. Haas, H. W. Zandbergen and R. J. Cava, Nature (London) **410**, 343 (2001).

[49] J. M. Ziman, *Principles of the Theory of Solids*, (Cambridge: Cambridge University Press, 1972), p.211

[50] C. U. Jung, Heon-Jung Kim, Min-Seok Park, Mun-Seog Kim, J. Y. Kim, Zhonglian Du, Sung-Ik Lee, K. H. Kim, J. B. Betts, M. Jaime, A. H. Lacerda, G. S. Boebinger, Physica **377**, 21 (2002).

[51] F. S. Razavi, private communication.

[52] S. K. Bose, private communication.

[53] Robert C. Weast, Samuel M. Selby, (*Handbook of Chemistry and Physics*, Cleveland: The Chemical Rubber Co., 1966).

[54] *Inorganic Index to the Powder Diffraction File* (Swarthmore [Pa]: Joint Committee on Powder Diffracion Standards, 1972).

[55] *Fink Index; The Powder Diffraction File*, (Swarthmore [Pa]: Joint Committee on Powder Diffracion Standards, 1972).

[56] *Powder diffraction file: inorganic volume*, (Swarthmore [Pa]: Joint Committee on Powder Diffraction Standards, 1960).

[57] A. Van Itterbeek, *Physics of High Pressures and the Condensed Phase*, (Amsterdam: Horth-Holland Publishing Company, 1956).

[58] R. S. Bradley, *High Pressure Physics and Chemistry*, (Glasgow: Academic Press, 1963).

[59] J. W. Garland, K. H. Benneman, *Superconductivity in d- and f-band metals. A.I.P. Conf. Proc. No. 4*, (New York: American Inst. of Physics, 1972), 255